NOZZLE FREE JET FLOWS WITHIN THE STRONG CURVED SHOCK REGIME

BY

TSO-SHIN SHIH

B.S., National Taiwan University, 1964
M.S., University of North Dakota, 1969

THESIS

Submitted in partial fulfillment of the requirements
for the degree of Doctor of Philosophy in Mechanical Engineering
in the Graduate College of the
University of Illinois at Urbana-Champaign, 1975

Urbana, Illinois

NOZZLE FREE JET FLOWS WITHIN THE STRONG CURVED SHOCK REGIME

BY

TSO-SHIN SHIH

B.S., National Taiwan University, 1964
M.S., University of North Dakota, 1969

THESIS

Submitted in partial fulfillment of the requirements
for the degree of Doctor of Philosophy in Mechanical Engineering
in the Graduate College of the
University of Illinois at Urbana-Champaign, 1975

Urbana, Illinois

NOZZLE FREE JET FLOWS WITHIN THE STRONG CURVED SHOCK REGIME

Tso-Shin Shih, Ph.D.
Department of Mechanical and Industrial Engineering
University of Illinois at Urbana-Champaign, 1975

A study based on inviscid analysis has been made to examine the flow field produced from a convergent-divergent nozzle when a strong curved shock occurs. It is learned that a certain constraint is imposed on the flow solution of the problem which is the unique feature of the flow within this flow regime and provides the reason why the inverse method of calculation cannot be employed for these problems. An approximate method has been developed to calculate the flow field and results have been obtained for two-dimensional flows. Analysis and calculations have also been performed for flows with axial symmetry. It is learned that under certain conditions, the vorticity generated at the jet boundary may become infinite and the viscous effect becomes important. Under other conditions, the asymptotic free jet height as well as the corresponding shock geometry have been determined.

ACKNOWLEDGMENT

The author wishes to express his sincere appreciation and gratitude to his advisor, Professor W. L. Chow, for his constant support and guidance through ideas, discussions, and direct assistance, without which this dissertation could not have taken its final form.

This work was supported by a research grant, NGL 14-005-140, from the National Aeronautics and Space Administration, Lewis Laboratory, Cleveland, Ohio, for which the author is deeply indebted.

Special thanks are due Mrs. June Kempka for her assistance in preparing the final manuscript.

The author is indebted to his parents and family, especially his wife and daughter for their patience, encouragement, and understanding.

TABLE OF CONTENTS

NOMENCLATURE

A,B,C,D	coefficients of ϕ function
M	Mach number
n,s	curvilinear coordinates measured normal to and along streamline
p	pressure
q	velocity
R	gas constant
S	entropy
t	time
u,v	velocity components in x- and y-directions
X,Y	Cartesian coordinates
X_s	shock profile
δ	shock turning angle
η	dimensionless normal coordinate
θ	stream angle
κ	ratio of specific heats, $\kappa = 1.4$ for air
ε	dimensionless horizontal coordinate
ρ	density
σ	shock angle
ϕ	velocity profile
ψ	stream function
ω	vorticity

Subscripts

a	asymptotic state conditions
c	evaluated at nozzle centerline
e	evaluated at nozzle exit plane

j	evaluated at free jet boundary
o	stagnation conditions
s	evaluated at curved shock

1. INTRODUCTION

The study of compressible flow through a convergent-divergent nozzle provides the most basic and fundamental knowledge of the flow of a compressible fluid. Depending upon the ambient pressure ratio (ambient to the supply pressure), a variety of flow patterns occurs both inside and outside the nozzle. While the flow inside the nozzle will be essentially unchanged for sufficiently low pressure ratios, the free jet flow patterns may be entirely different due to the existence of a family of oblique shock solutions. These flow phenomena may be further complicated by the fact that the real fluid is viscous and the flow may separate (shock induced separation) from the solid wall inside the nozzle when the wall boundary layer cannot cope with the high ambient pressure prevailing outside the nozzle. One should recognize, however, that in order to understand the viscous effect on the overall flow pattern, it is a prerequisite that the flow solution based on purely inviscid analysis be established.

In the major operating range of the nozzle pressure ratios, the inviscid flow patterns of the free jet flow are relatively simple, and the description of them can be found in standard text books [1,2,3].* There exists, however, a range of the pressure ratios where the inviscid free jet flow patterns are very complicated and have not been established.

Referring to Fig. 1 where a series of two-dimensional nozzle free jet flow is depicted, an oblique shock is generated from the edge of the nozzle when the ambient pressure p_a is kept slightly above the exit pressure p_e. This shock can be regularly reflected from the centerline (Fig. 1a) if the strength of the incident shock is not strong enough to prevent the occurrence of such a reflection. For higher pressure ratios where such a

*Numbers in brackets refer to entries in REFERENCES.

regular reflection is not possible, Mach reflection may occur within the flow field (Fig. 1b). Recent studies by Chang [4] and Chow and Chang [5,6] on Mach reflection of shock and Mach disc showed that for small nozzle Mach numbers ($M_N < 1.484$ for $\kappa = 1.4$), Mach reflection cannot occur since the triple point condition based on inviscid analysis cannot be satisfied. For larger nozzle Mach numbers, Mach reflection of shock is possible and the Mach stem height will be increased for higher pressure ratios. Even in this situation, there exists a range of nozzle Mach numbers where the Mach stem height can never reach the height of the nozzle for sufficiently high pressure ratios and a strong curved shock necessarily occurs in the flow field (Fig. 1c).

Perhaps the above description of the flow events may be best illustrated in Figs. 2, 3, and 4. Figure 2 shows the possible conditions for the occurrence of a triple point (Mach reflection pattern) and various limits for shock reflection. It is also recognized that from inviscid considerations no triple point can occur for $M_N < 1.484$ ($\kappa = 1.4$). Figure 3 illustrates the Mach stem height calculated by either detailed calculations or by approximate method corresponding to different operating conditions. It may be seen that for moderate supersonic nozzle Mach numbers, the maximum Mach stem height is still smaller than the height of the nozzle. Figure 4 illustrates the corresponding pressure ratio when Mach reflection occurs. It is now obvious that for pressure ratios higher than those required for Mach reflection (or regular reflection for $M < 1.65$) but lower than the corresponding normal shock values, the regime of strong curved shock prevails.* Under this condition, a shock wave

*This regime may overlap that of Mach reflection.

(which may even belong initially to the weak shock solution) is generated at the corner of the nozzle (Fig. 1c) and proceeds downstream with increasing wave angle and shock strength until the normal shock condition is attained on the centerline of the nozzle. This shock is never reflected, and the downstream flow field is bounded by a constant pressure boundary. The majority of the flow field is subsonic. Since the curved shock generates vorticity, the flow is thus rotational. Eventually all streamtubes are straight and parallel to the nozzle centerline so that the pressure becomes uniform and is equal to the ambient pressure. However, the velocity, density, etc., are non-uniform which is, of course, the result of the existence of the vorticity. This state--termed the asymptotic state--can exist only at the mathematically "far downstream" positions.

It should be pointed out that in previous studies [4,5,6] on the occurrence of triple point, inviscid considerations were found to be adequate from experimental observations made with a shock tube [7] for relative strong incident shocks. However, for weak incident shocks (small Mach number and small shock strength), triple point has been observed [7] under conditions even when the inviscid analysis does not yield a solution. It is conceivable that under these conditions, the thickness of the shock wave may not be thin enough that its subsequent interaction with the flow fields may become an important point of consideration for the solution at the triple point. In view of these observations [7], the range of occurrence of Mach reflection presented by Chow and Chang may not be precise; nevertheless, it provides useful guidance in describing the flow regimes of free jet flow under different operating conditions.

While the existence of such a strong curved shock flow regime has been mentioned only briefly by Ferri [2], no work has been performed in

the study of associated free jet patterns within this flow regime. It is true that all nozzles do not normally operate under such flow conditions and even they do, the viscous effects may significantly modify the flow pattern. The motivation of studying such flow problems comes not only from filling the gap of information which, so far, is lacking. The unique character of such a rotational subsonic or mixed flow field downstream of a curved strong shock and extending to far downstream positions offers considerable interest and challenge. It should be reiterated that a flow solution, on the basis of purely inviscid flow analyses, should be established before any viscous effects can be incorporated into the considerations. This is indeed the purpose of the present investigation.

Since the problem under consideration concerns the determination of the profile of a strong curved shock and the details of the free jet flow behind it, it is similar to the blunt body problem, i.e., a blunt body immersed in a supersonic flow with a detached shock wave. The method of analysis for the blunt body problem will be reviewed.

The blunt body problem has been a matter of concern since early 1950, and many methods for solving problems of this type have been developed. These methods of approach may be classified as solutions to direct or inverse problems. For the direct problem, the shape of the body is given while the shock profile and details of the flow field between the shock and body are to be examined. In the inverse problem, the shock shape is specified and the resulting body configuration and accompanying velocity and pressure fields on, or ahead of, the body are to be calculated. These different methods of analysis are discussed in the following section.

For the direct problem, the analyses usually can be divided into (1) the method of integral relations, (2) the unsteady flow approach, and

(3) the relaxation method. The method of integral relations was originally developed by Dorodnitsyn [8] as a general method of numerical solution for nonlinear hydrodynamic problems. It reduces the problem of integrating a system of nonlinear partial differential equations to that of solving an approximate system of ordinary differential equations. This method was originally applied to the blunt body problem by Belotserkovskii [9] to calculate the supersonic flow of a perfect gas past a circular cylinder. Following this method of approach, many calculations for more general body shapes in symmetric flows have also appeared [10].

The use of the method of integral relations was also proposed by Mel'mikov [11] for calculating the flow behind the Mach stem of an over-expanded supersonic nozzle where Mach reflection occurs. For the case of a single strip, a system of ordinary differential equations with corresponding boundary conditions describing the problem was derived. However, no numerical results were obtained.

In the unsteady flow method, the steady flow solution is obtained as the limiting state is reached asymptotically in time from an unsteady flow with constant free stream and body conditions and suitably chosen initial conditions. The unsteady flow equations are solved by finite difference techniques. Von Neumann and Richtmeyer [12] first suggested this idea to calculate one-dimensional flow associated with shocks. In their calculation, large computer storage is required and, as a result of the shock not being considered as a sharp discontinuity, the computational time is too lengthy. Later, Von Neumann and Richtmeyer's idea was developed and extended by Lax and Wendroff [13] and others. By properly setting the equations into finite difference form, solutions may be obtained in which

shock waves are approximated by narrow regions where the physical parameters undergo drastic changes. Moretti and Abbett [14] further improved this method by introducing special three-dimensional method of characteristics to describe the conditions on the shock and body boundaries. The points between shock and body were calculated by employing the technique developed by Lax and Wendroff. This method has also been extended to calculate the three-dimensional steady flows by Moretti and Bleich [15].

In the relaxation method, a stream function is usually introduced as a dependent variable. The differential equation for the stream function is considered as the basic equation. The plane for numerical calculations is covered by a network of squares. The basic differential equation is written in finite difference form and a residue which must be zero everywhere when the final solution is reached is defined at each point. The assumed values of the dependent variables are then substituted into these equations. In general, the residue which is a measure of the failure of the assumed solution to satisfy the equation will not be zero. The problem is to reduce by suitably adjusting the assumed values of the dependent variables the residuals to zero at every point. Gravalos, Edelfelt, and Emmons [16] and Hayes and Probstein [17] used this method to calculate the blunt body problem.

In the inverse problem, the shape of the detached shock is assumed and the numerical calculations are subsequently carried out until the body whose geometry is obtained by locating the points corresponding to constant stream functional values (e.g., $\psi = 0$) is reached. One may observe that the resulting body shape corresponds to the selected detached shock geometry. However, fundamental questions arise with respect to the uniqueness and the existence of a solution with respect to the stability

convergence of calculation procedures. Hayes and Probstein [17] stated:

> "the most important single feature of this inverse problem is the insensitiveness of the shock shape to local changes in the body shape, and this feature leads to essential difficulties in the inverse problem. A minute local change in the shock shape will generally cause a large change in the body shape and may even preclude the existence of a solution."

From a mathematical point of view, they also stated:

> "the determination of the subsonic part of the flow field in the problem is governed by an elliptic partial differential equation"

and

> "we know as far as elliptic differential equations are concerned, the initial value problem is improperly posed and leads to an unstable solution when treated by finite difference."

However, the inverse problem was solved successfully by several authors [18,19,20] who found that suitable numerical methods would yield sufficiently accurate results even though such methods have regions of numerical instability.

It is now appropriate to point out that for blunt body problems, the elliptic region is finite. The flow will pass through a sonic line and become supersonic somewhere along the body. This may be the reason that, even when numerical instability and insensitivity of shock to body shapes exit, indirect problems can be calculated successfully. For the present problem, the elliptic region extends to infinity and is thus unbounded. It will be seen that application of such an inverse method, i.e., guessing a shock shape and "marching downstream," would be completely unworkable; in fact, it is doomed to fail.

Since the present flow regime of curved strong shock is identified only after the phenomenon of Mach reflection is understood, it is also necessary to describe briefly the work by Chow and Chang [6] on Mach reflection. It was recognized that when Mach reflection occurs, the central core flow will pass through a strong shock (Mach shock) while the fluid above it will go through relatively weak incident and reflected shocks. Since it is necessary that these two portions of the fluid assume the same pressure and same streamline flow angle along the common boundary, it is obvious that the mutual interaction between the streams plays the controlling role to the solution of the problem. It was shown that for supersonic flow state behind the reflected shock, the core flow will eventually pass through a throat-like condition similar to the choked secondary flow within the supersonic ejector system [21]. The detailed calculations of the flow field, including the determination of the Mach stem height, may be performed with the method of characteristics for the upper stream and with the simplified one-dimensional analysis for the core flow after the method of integral relations has been applied for both streams. However, when the state behind the reflected shock is subsonic, such detailed calculations are not possible and the Mach stem is estimated from an approximate method stressing the interacting force between two streams. These considerations have also been extended into axisymmetric flow configurations. Some of these results are presented in Figs. 2, 3, and 4; other results were reported by Chang [4] and by Chow and Chang [6].

2. THEORETICAL CONSIDERATIONS

2.1 DESCRIPTION OF THE PROBLEM

On the basis of the discussion presented in the preceding chapter, it is recognized that the present problem occurs for a supersonic flow issuing from a nozzle when the ambient pressure is high enough that an oblique shock is generated at the corner of the nozzle. The wave angle of the shock increases as it moves downstream until a normal shock is attained on the centerline of the nozzle. The flow behind the shock is bounded on one side by a constant pressure free jet boundary and is rotational. The viscous effects occuring along the jet boundary and within the fluid are disregarded. Eventually, all streamlines become parallel to the axis of symmetry, and the pressure is equal to the ambient value. The velocity, however, is non-uniform at this asymptotic state as a result of the presence of vorticity. A schematic diagram depicting such a flow field is shown in Fig. 5. Since the flow is symmetric with respect to the x-axis, only one-half of this region will be considered.

2.2 BASIC RELATIONS GOVERNING THE FLOW

One now proceeds to formulate the problem in a more detailed and precise manner. The governing relations are listed sequentially in the following sections.

2.2.1 Shock Relations

For the occurrence of an oblique shock within a supersonic flow field, the governing algebraic equations are:

$$\frac{p_s}{p_e} = \frac{2\kappa}{\kappa + 1} M_e^2 \sin^2 \sigma - \frac{\kappa - 1}{\kappa + 1} \tag{2.1}$$

$$\tan \delta = 2 \cot \sigma \frac{M_e^2 \sin^2 \sigma - 1}{M_e^2 (\kappa + \cos 2\sigma) + 2} \tag{2.2}$$

$$\frac{\rho_s}{\rho_e} = \frac{\tan \sigma}{\tan (\sigma - \delta)} \tag{2.3}$$

$$\frac{u_s}{u_e} = \frac{\cos \sigma \cos \delta}{\cos (\sigma - \delta)} \tag{2.4}$$

$$\frac{v_s}{u_e} = \frac{\cos \sigma \sin \delta}{\cos (\sigma - \delta)} \tag{2.5}$$

2.2.2 Free Jet Flow Region

For a two-dimensional inviscid flow of a compressible fluid, the continuity and momentum principles can be given as:

(Hereafter, unless mentioned otherwise, all fluid properties will be treated as normalized by the corresponding values at the nozzle exit condition, and all length quantities are normalized by the half-height of the nozzle.)

$$\frac{\partial \rho u}{\partial x} + \frac{\partial \rho v}{\partial y} = 0 \tag{2.6}$$

$$\rho u \frac{\partial u}{\partial x} + \rho v \frac{\partial u}{\partial y} = - \frac{1}{\kappa M_e^2} \frac{\partial p}{\partial x} \tag{2.7}$$

$$\rho u \frac{\partial v}{\partial x} + \rho v \frac{\partial v}{\partial y} = - \frac{1}{\kappa M_e^2} \frac{\partial p}{\partial y} \tag{2.8}$$

The energy equation can be given simply as

$$\frac{DS}{Dt} = 0 \tag{2.9}$$

where S denotes entropy. It is understood that due to the curved shock prevailing upstream, the flow field is not homentropic. Nevertheless, the flow is isentropic along individual streamlines. This would also imply that the flow is isoenergetic throughout the field.

The flow region under consideration is bounded by (1) a constant pressure jet boundary whose profile, $y_j(x)$ is yet unknown, (2) a line of symmetry which is the x-axis, (3) the upstream curved shock whose shape, $x_s(y)$, is also unknown, and (4) the asymptotic state prevailing at far downstream position (i.e., $x \to \infty$). The boundary conditions imposed on the solution of Eqs. (2.6), (2.7), and (2.8) are:

$$p = p_a \qquad \text{along } y_j(x) \tag{2.10}$$

$$\left.\begin{aligned} u &= u_s \\ v &= v_s \\ p &= p_s \\ \rho &= \rho_s \end{aligned}\right\} \qquad \text{along } x_s(y) \tag{2.11}$$

and

$$v = 0, \ \frac{\partial u}{\partial y} = 0 \text{ at } y = 0 \tag{2.12}$$

In addition, any solution corresponding to a particular ambient pressure ratio must be subjected to a certain constraining condition when the asymptotic state is reached. This is considered in detail in the next section.

2.2.3 Constraining Condition at the Asymptotic State

One now gives attention to the control volume shown in Fig. 6a. The continuity principle would yield

$$\int_0^{y_{aj}} \rho_a \, u_a \, dy = \rho_e \, u_e \, y_e = 1 \tag{2.13}$$

The x-momentum principle also gives

$$\int_0^{y_{aj}} \rho_a \, u_a^2 \, dy + \frac{1}{\kappa \, M_e^2} \, p_a \, y_e = \frac{1}{\kappa \, M_e^2} \, p_e \, y_e + \rho_e \, u_e^2 \, y_e \tag{2.14}$$

which can be rewritten as

$$\int_0^{y_{aj}} \rho_a \, u_a^2 \, dy = 1 - \frac{1}{\kappa \, M_e^2} \, (p_a - 1) \tag{2.15}$$

It should be noted that for the present problem, the right-hand side of Eq. (2.15) is a constant value which is greater than zero but less than unity.

After introducing ρ_{aj}, u_{aj}, and y_{aj} as reference quantities for the integrands in Eqs. (2.13) and (2.15) and defining $\phi = u_a/u_{aj}$ and $\eta = y/y_{aj}$, these equations become

$$\rho_{aj} \, u_{aj} \, y_{aj} \int_0^1 \frac{\rho_a}{\rho_{aj}} \, \phi \, d\eta = 1 \tag{2.16}$$

$$\rho_{aj} \, u_{aj}^2 \, y_{aj} \int_0^1 \frac{\rho_a}{\rho_{aj}} \, \phi^2 \, d\eta = 1 - \frac{1}{\kappa \, M_e^2} \, (p_a - 1) \tag{2.17}$$

Upon combining Eqs. (2.16) and (2.17), one obtains

$$\int_0^1 \frac{\rho_a}{\rho_{aj}} \, \phi^2 \, d\eta = \frac{1 - \frac{1}{\kappa \, M^2} \, (p_a - 1)}{u_{aj}} \int_0^1 \frac{\rho_a}{\rho_{aj}} \, \phi \, d\eta \tag{2.18}$$

which is equivalent to

$$\int_0^1 \frac{\rho_a}{\rho_{aj}} \phi \left(\phi - \frac{1 - \frac{1}{\kappa M^2} (p_a - 1)}{u_{aj}} \right) d\eta = 0 \tag{2.19}$$

where ρ_a/ρ_{aj} is related to ϕ through

$$\frac{\rho_a}{\rho_{aj}} = \frac{1 - C_{aj}^2}{1 - C_{aj}^2 \phi^2} \tag{2.20}$$

and C_{aj} is a constant for a particular nozzle Mach number operating under a particular pressure ratio. It should be noted that the two integrals have positive definite integrands which are never greater than unity as ϕ varies from ϕ_c ($\phi_c = u_{ac}/u_{aj} < 1$) to unity; thus,

$$\int_0^1 \frac{\rho_a}{\rho_{aj}} \phi \, d\eta \geq \int_0^1 \frac{\rho_a}{\rho_{aj}} \phi^2 \, d\eta$$

and

$$\phi_c \leq \frac{1 - \frac{1}{\kappa M_e^2} (p_a - 1)}{u_{aj}} \leq 1.$$

Equation (2.19) provides the constraining condition of the flow when the asymptotic state is reached which in turn imposes the additional condition which the solution of the problem must satisfy.

It is now clear that this constraint is the reason that the indirect approach to the blunt body problem cannot be adopted for the present calculations. The hope of estimating a curved shock profile and marching downstream and correcting the upstream shock shape from some unmatched properties prevailing downstream can never be realized. If a certain shock shape is assumed, it immediately determines the corresponding asymptotic state for each of the stream tubes. Usually this profile will not satisfy

the constraining condition given by Eq. (2.19). Marching downstream with such a shock will necessarily result in illogical mathematic operations (e.g., seeking the square root of a negative number) if these calculations were performed on a digital computer and the computation was interrupted before the asymptotic state was reached. Since an accurate estimation of the shock shape* is impossible, such interruption can never be avoided. This explains why the indirect method cannot be applied to the present problem.

A method has been devised and is suggested to solve the present flow problem. It is recognized that with a given nozzle operating at a particular pressure ratio within this flow regime, the asymptotic conditions of the jet boundary and center streamlines are known. A velocity profile at the asymptotic state which, in addition to fulfilling all required boundary conditions, contains one additional parameter which is to be determined by the constraining relations given by Eq. (2.19). Once the asymptotic profile and thus y_{aj} are determined, the associated upstream curved shock geometry can be evaluated and the flow field between the shock and the asymptotic state can be determined through numerical calculations.

2.3 ASYMPTOTIC STATE

Since the solution of the problem relies on the establishment of the asymptotic flow profile, a detailed examination of the conditions imposed on such an asymptotic flow state is therefore necessary.

---

*It is believed that even if the correct shock shape were inserted upstream, the subsequent error of calculations due to round-off or truncation would eventually cause the termination of calculations.

Under the asymptotic flow condition, the slope of the velocity profile is precisely the vorticity of the flow. A study of the vorticity generated by the shock* at the corner of the nozzle would also yield the slope of the profile of the jet boundary streamline at the asymptotic state.

2.3.1 Vorticity at the Jet Boundary Streamline

One now examines the flow condition (downstream of the shock) at the corner of the nozzle where the shock is generated (Fig. 7). In the streamline coordinate system, the continuity equation is given in dimensional form by:

$$\frac{1 - M_e^2}{q} \frac{\partial q}{\partial s} + \frac{\partial \theta}{\partial n} = 0, \tag{2.21}$$

and the equations of motion for the s and n directions are, respectively:

$$q \frac{\partial q}{\partial s} = - \frac{1}{\rho} \frac{\partial p}{\partial s}, \tag{2.22}$$

and

$$\rho q^2 \frac{\partial \theta}{\partial s} = - \frac{\partial p}{\partial n} \tag{2.23}$$

where θ is the streamline angle and q is the velocity of the fluid. The vorticity can also be expressed by

$$\omega = \frac{\partial q}{\partial n} - q \frac{\partial \theta}{\partial s} = \frac{p}{\rho q R} \frac{\partial S}{\partial n}. \tag{2.24}$$

For a jet boundary streamline at the corner of the nozzle, Eq. (2.21) implies $\partial\theta/\partial n\big|_j = 0$ as $\partial p/\partial s = 0$. It may be seen that

$$\omega_j = \frac{p}{\rho q R} \frac{\partial S}{\partial n} = \frac{p}{\rho q R} \left(\frac{dS}{d\sigma} \frac{d\sigma}{d\theta} \frac{\partial \theta}{\partial n} \right) = 0. \tag{2.25}$$

*The infinite vorticity due to the discontinuous change in velocity at the jet boundary is, of course, not under consideration.

It is thus recognized that vanishing vorticity occurs along the jet boundary, implying that the slope of the velocity profile at the asymptotic state should vanish at the jet boundary.

2.3.2 Velocity Profile at the Asymptotic State

One now realizes that this velocity profile ϕ in Eq. (2.19) should satisfy the conditions

(i) At $\eta = 0$:

$$\phi = \phi_c = \frac{u_{ac}}{u_{aj}} \text{ and } \frac{d\phi}{d\eta} = 0 \tag{2.26}$$

(ii) At $\eta = 1$:

$$\phi = 1 \text{ and } \frac{d\phi}{d\eta} = 0 \tag{2.27}$$

In view of the simple requirements to be satisfied by such a profile, many functions seem to satisfy the need of the present analysis. It should be noted that it is not a simple matter to select such a profile. It is pointed out that a very stringent requirement which has not been presented herein is that the curvature (or $d^2\phi/d\eta^2$) of the profile should be non-negative at $\eta = 0$ for the whole range of the pressure ratios. As no physically possible flow situation can occur under the condition when $d^2\phi/d\eta^2\Big|_{\eta=0}$ is negative, it has been found that polynomials, sine, and cosine functions, cannot meet this requirement throughout the range of pressure ratios.

A profile has been selected which has the following form:

$$\phi = A + B \text{ erf } [C (1 - \eta^2)] + D \text{ erf } [C (1 - \eta^4)] \tag{2.28}$$

where A, B, and D are parameters to be determined from conditions given by Eqs. (2.26) and (2.27). Only even powers of η appear in the above equation due to the condition of symmetry. Upon evaluating these parameters, Eqs. (2.28) becomes:

$$\phi = 1 - \frac{2\,(1 - \phi_c)}{\text{erf}\ (C)}\ \text{erf}\ [C\,(1 - \eta^2)] + \frac{1 - \phi_c}{\text{erf}\ (C)}\ \text{erf}\ [C\,(1 - \eta^4)] \qquad (2.29)$$

The coefficient C is yet to be determined for each particular pressure ratio so that the constraining relationship, Eq. (2.19), can be satisfied. A range of values of C has been found for different nozzle Mach numbers under various pressure ratios and is given in Table 1.

Once the value of C is determined from the constraining condition, the free jet height y_{aj} at this position can also be computed and the detailed shape of the asymptotic profile completely established. This information would readily lead to the determination of the geometry and the strength of the upstream curved shock wave. Some of these typical velocity profiles are presented in Fig. 9.

2.4 CORRESPONDING UPSTREAM SHOCK PROFILE

After the asymptotic height of the free jet, y_{aj}, and its detailed profile are established, the corresponding curved shock configuration can be determined through the following considerations: (Also, see Fig. 6b.) If one carries out the integration

$$\int_0^{y_a} \rho_a\ u_a\ dy \qquad (2.30)$$

along the asymptotic profile, the continuity principle would imply that the fluid assuming the position y_a at the asymptotic section would have passed through the shock at height y_s which is equal to

$$y_s = \int_0^{y_a} \rho_a\ u_a\ dy \qquad (2.31)$$

since the velocity of the fluid at y_a has a known value ϕ_a, its stagnation

pressure p_{oa} can be found from

$$\frac{p_{oa}}{p_a} = \left(\frac{1}{1 - C_{aj}^2 \, \phi_a^2} \right)^{(\kappa/\kappa-1)} \tag{2.32}$$

The ratio of the stagnation pressures across the shock at y_s can be related through the shock wave angle σ by

$$\frac{\left(\frac{\frac{\kappa+1}{2} M_e^2 \sin^2 \sigma}{1 + \frac{\kappa+1}{2} M_e^2 \sin^2 \sigma} \right)^{(\kappa/\kappa-1)}}{\left(\frac{2\kappa}{\kappa+1} M_e^2 \sin^2 \sigma - \frac{\kappa-1}{\kappa+1} \right)^{1/\kappa-1}} = \frac{p_{oa}}{p_{oe}} = \frac{p_{oa}}{p_a} \frac{p_a}{p_{oe}} \tag{2.33}$$

where p_a/p_{oe} is the operating pressure ratio.

Thus, the wave angle σ can be found as a function of any position y_s along the shock. Additional integration of the relationship

$$\frac{dy_s}{dx} = \tan \sigma \tag{2.34}$$

with the initial condition of $x_s = 0$, $y_s = 1$ would produce the shock configuration $x_s(y_s)$ corresponding to the established asymptotic profile.

2.5 FLOW FIELD BETWEEN THE SHOCK AND THE ASYMPTOTIC STATE

One now proceeds to investigate the detailed flow field between the curved shock and the final asymptotic state. The basic differential equations governing the flow are rewritten as:

$$\rho \left(\frac{\partial u}{\partial x} + \frac{\partial v}{\partial y} \right) + u \frac{\partial \rho}{\partial x} + v \frac{\partial \rho}{\partial y} = 0 \tag{2.6}$$

$$\rho \left(u \frac{\partial u}{\partial x} + v \frac{\partial u}{\partial y} \right) = - \frac{1}{\kappa M_e^2} \frac{\partial p}{\partial x} \tag{2.7}$$

$$\rho\left(u\frac{\partial v}{\partial x}+v\frac{\partial v}{\partial y}\right)=-\frac{1}{\kappa M_e^2}\frac{\partial p}{\partial y} \tag{2.8}$$

For the convenience of numerical calculations, another pair of independent variables, ξ and ψ, which are related with x and y coordinates through

$$\xi=\frac{x-x_s(\psi)}{1+x-x_s(\psi)} \tag{2.35}$$

$$\frac{\partial\psi}{\partial x}=-\rho v \text{ and } \frac{\partial\psi}{\partial y}=\rho u \tag{2.36}$$

are introduced. ψ is the dimensionless stream function and x_s, which can easily be interpreted as a function of ψ, is the upstream curved shock configuration. Upon adopting this pair of independent variables, the semi-infinite physical region is transformed into a rectangular finite domain in the ξ,ψ plane. Lines of constant ψ values correspond to streamlines, shock corresponds to $\xi = 0$, and $\psi = 1$ corresponds to the free jet boundary. The asymptotic state assumes the location $\xi = 1$ (see Fig. 8).

It may easily be established that the transformational relations are:

$$\left.\frac{\partial}{\partial x}\right|_y=(1-\xi)^2\left(1+\rho v\frac{dx_s}{d\psi}\right)\frac{\partial}{\partial\xi}-\rho v\frac{\partial}{\partial\psi} \tag{2.37}$$

and

$$\left.\frac{\partial}{\partial y}\right|_x=(1-\xi)^2\rho u\frac{dx_s}{d\psi}\frac{\partial}{\partial\xi}+\rho u\frac{\partial}{\partial\psi} \tag{2.38}$$

and Eqs. (2.6), (2.7), and (2.8) become

$$(1-\xi)^2\rho\left(1+\rho v\frac{dx_s}{d\psi}\right)\frac{\partial u}{\partial\xi}-\rho^2 v\frac{\partial u}{\partial\psi}-(1-\xi)^2\rho^2 u\frac{dx_s}{d\psi}\frac{\partial v}{\partial\xi}$$

$$+\rho^2 u\frac{\partial v}{\partial\psi}+(1-\xi)^2 u\frac{\partial\rho}{\partial\xi}=0 \tag{2.39}$$

$$(1 - \xi)^2 \rho u \frac{\partial u}{\partial \xi} + \frac{1}{\kappa M_e^2} (1 - \xi)^2 \left(1 + \rho v \frac{dx_s}{d\psi}\right) \frac{\partial p}{\partial \xi} - \frac{1}{\kappa M_e^2} \rho v \frac{\partial p}{\partial \psi} = 0 \tag{2.40}$$

$$(1 - \xi)^2 \frac{\partial v}{\partial \xi} - \frac{1}{\kappa M_e^2} (1 - \xi)^2 \frac{dx_s}{d\psi} \frac{\partial p}{\partial \xi} + \frac{1}{\kappa M_e^2} \frac{\partial p}{\partial \psi} = 0 \tag{2.41}$$

In addition, the isoenergetic condition is given by

$$\frac{1}{\kappa - 1} \frac{1}{M_e^2} \frac{p}{\rho} + \frac{u^2 + v^2}{2} = \frac{1}{2} + \frac{1}{\kappa - 1} \frac{1}{M_e^2} \tag{2.42}$$

The isentropic flow relationship along individual streamlines can be written as

$$\frac{p}{\rho^\kappa} = f(\psi) \tag{2.43}$$

where $f(\psi)$ is evaluated according to the already established shock conditions.

It may be observed that the asymptotic flow condition which may be given as

$$p = p_a, \quad v = 0, \quad \frac{\partial p}{\partial \xi} = 0, \quad \frac{\partial p}{\partial \psi} = 0$$

$$\frac{\partial u}{\partial \xi} = 0, \quad \frac{\partial v}{\partial \xi} = 0, \quad \text{and} \quad \frac{\partial v}{\partial \psi} = 0 \text{ at } \xi = 1 \tag{2.44}$$

satisfies Eqs. (2.39), (2.40), and (2.41) identically.

The boundary conditions for the system of equations are:

(1) At $\xi = 0$, all flow properties are provided from the shock relations given by Eqs. (2.1) through (2.5). (2.45)

(2) At $\xi = 1$, all flow properties are provided from the asymptotic state. (2.46)

(3) At $\psi = 1$, $p = p_a$, and $\rho = \rho_{aj}$. (2.47)

(4) At $\psi = 0$, $v = 0$, $\partial p/\partial \psi = 0$, $\partial u/\partial \psi = 0$, and $\partial \rho/\partial \psi = 0$. (2.48)

2.5.1 Numerical Calculations

A predictor-corrector finite difference method has been applied to solve numerically the above partial differential equations (i.e., Eqs. (2.39), (2.40), and (2.41)) with the corresponding boundary conditions given by Eqs. (2.45), (2.46), (2.47), and (2.48). In order to carry out the numerical calculations, the square ABCD in the ξ,ψ plane has been divided into small meshes as shown in Fig. 8c.

In the predictor phase of the numerical method, flow properties ρ, u, and v within the region are estimated. The pressure can always be related with these ρ, u, and v values through the isoenergetic condition or the isentropic relationship when its ψ value is known. To obtain the initial information of ρ, u, and v, their values along the $\xi = 0.5$ line is established initially by obtaining:

(1) The ρ_ξ, u_ξ, and v_ξ* values from the standard three-point central difference scheme from the known values of properties at $\xi = 0$ and $\xi = 1$,

(2) The ρ_ψ, u_ψ, and v_ψ values from the basic equations, and

(3) Integration of these derivatives from $\psi = 1$ toward $\psi = 0$ numerically by applying the formula of

$$f(\psi - \Delta\psi) = f(\psi) - \frac{\partial f}{\partial \psi}(\psi)\,\Delta\psi \tag{2.49}$$

where f denotes any representative property of the fluid.

Initial values of u (or v) at $\psi = 1$ must be adjusted so that the condition

$$v_{(\psi=0)} = 0 \tag{2.50}$$

is satisfied on the axis.

---

*Subscripts now indicate differentiation.

These processes are repeated for constant ξ lines between $0 < \xi < 0.5$ and $0.5 < \xi < 1.0$.

In the corrector phase of the calculations, values of ρ, u, and v are recalculated by following the same procedures but using the standard five-point central difference formula [22] in ξ derivatives and the three-point central difference in ψ derivatives* starting from the $\xi = 0.5$ line. In correcting the property values from the $\psi = 1$ line toward the axis ($\psi = 0$), a more sophisticated local predictor-corrector technique [20] has been applied. These correcting calculations should be repeated until the differences of the fluid property between the successively determined values of all node points in the ξ,ψ plane are within a desirable limit. In this study, this limit is taken as 10^{-6}.

Once the final flow properties are determined, including those along the jet boundary, the profile of the jet may be established by integrating the expression $dy_j/dx_j = v_j/u_j$ with the initial condition of $y_j = 1$ at $x = 0$.

2.6 DEGENERATE STATE

It should be pointed out that for each nozzle Mach number, there exists a pressure ratio corresponding to the normal shock appearing at the exit section of the nozzle. The downstream flow field is uniform (i.e., $y_j \equiv 1$) and the constraining condition becomes the Rankine-Hugoniot relationship which is automatically satisfied by the normal shock. Such a state is termed the "degenerate state" and the corresponding pressure ratio for its appearance is presented in Fig. 4.

---

*This must be modified for the lines adjacent to shock, the asymptotic state, and the $\psi = 1$ and $\psi = 0$ streamlines.

3. RESULTS AND DISCUSSION

The method described in the previous chapter has been translated into a FORTRAN IV computer program with double precision. For a given initial Mach number at a certain operating pressure ratio, it takes approximately five seconds of computational time on the IBM 360/75 digital computer to calculate all flow properties related to the problem. In this study, cases of three initial Mach numbers (M_e = 1.49, 3.0, and 5.0) operating at different pressure ratios have been calculated. The results are plotted and presented in Figs. 9 through 18.

In Fig. 9, the calculated asymptotic velocity profiles ϕ are plotted against the coordinate η. It can be seen from those profiles that the change of ϕ from ϕ_c to unity occurs mainly in the upper part of η. This is especially true for higher pressure ratios and also true for higher nozzle Mach numbers. From Table 1 it can be seen that the coefficient C of ϕ function (Eq. (2.29)) has larger values at higher pressure ratios. This explains why the core flow is essentially uniform under these flow conditions.

The results of the free jet flow calculated by predictor-corrector scheme also shows that when the operating pressure ratio is sufficiently high, there is a uniform core flow around the centerline. The portion of this uniform core flow increases as the pressure ratio is increased. When the normal shock pressure ratio is reached, the entire free jet flow becomes uniform.

The calculated centerline pressure variation and the free jet boundary profile are plotted against the x coordinate in Figs. 10 and 11. As the operating pressure ratio increases toward normal shock pressure ratio, the following phenomena have been observed:

(1) The value of shock stand-off distance x_{sc}, shown in Fig. 12, is reduced toward zero as the normal shock condition is approached.

(2) The corresponding asymptotic free jet boundary height, y_{aj}, increases toward unity.

(3) The practical distance, x_a, for the free jet flow to reach the asymptotic flow conditions is also reduced.

The pressure distribution and its variation throughout the field corresponding to specific flow conditions are shown in Fig. 13. Example to illustrate the differences in flow properties between the initial predicted value and final corrected values at $\xi = 0.5$ are presented in Figs. 14 and 15.

It should be mentioned that the asymptotic velocity profile represented by equation ϕ is certainly not the only type which can be adopted for the present problem. In a different effort, a profile of the form given by

$$\phi_1 = 1 - \frac{2\,(1 - \phi_c)}{\tanh\,(c)} \tanh\,[c\,(1 - \eta^2)] + \frac{1 - \phi_c}{\tanh\,(c)} \tanh\,[c\,(1 - \eta^4)] \tag{3.1}$$

has been employed, and the results are shown in Fig. 16. It can be seen that the difference between the ϕ_1 and ϕ profiles under the same condition is indeed small, and this small difference has also been observed under various pressure ratios. However, if one adopts a polynomial profile of the form

$$\phi_2 = A + B\,\eta^2 + C\,\eta^4 + D\,\eta^6, \tag{3.2}$$

it is found that the behavior of this profile is quite different from that of ϕ or ϕ_1 at the same pressure ratios. In fact, when a certain level of

pressure is reached, the profile has an absolute minimum velocity ocurring not at the centerline which does not correspond to any physically realistic flow condition (see Fig. 17). This is why the profile of a simpler form given by equation ϕ_2 has not been employed for the present study.

The solution of the problem, nevertheless, relies on the selection of the type of asymptotic profile. Although profiles of a similar nature may be adopted for this study, and the final results are not much different from each other, these solutions can be considered as only approximate solutions. Meanwhile, the selection of the profile in its present form, which is monotonically increasing for increasing y_a values, has dismissed the possibility of profiles with negative slope (positive vorticity) away from the centerline, whose occurrence may seem to be improbable but cannot be ruled out by any basic principles. In this sense, the selection of the asymptotic profile in its present form is somewhat restrictive.

Perhaps it is due to the restrictive character of the profile that some numerical instability of the results has been observed. In numerical calculations by finite difference schemes, it is generally recognized that for better definition or resolution of the flow field, finer grid should be employed. In the present study, a small step of η ($\Delta\eta = 0.01$) has been employed for calculations since it is needed especially in the region close to the centerline where normal shock occurs. However, all results reported here were obtained with $\Delta\xi = 0.125$. Finer grid size in the ξ direction has led to oscillatory flow results. Figure 18 shows one set of these results for the pressure distribution along the centerline when a smaller $\Delta\xi$ ($\Delta\xi = 0.0625$) is employed. It is thus obvious that with

the same numerical limit of 10^{-6} as the margin for convergence, a grid finer than $\Delta\xi = 0.0625$ may not even lead to convergent solutions.

It should also be mentioned that the question of how this curved shock flow regime merges with the regime of Mach reflection cannot be answered in this investigation. Additional study or even experimental explorations are needed before the problem can be resolved successfully.

Similar considerations can be applied to axisymmetric flow configurations within this curved shock flow regime. A detailed study and results are reported in the appendix. It should be noted that with the axisymmetric geometry, the vorticity along the jet boundary is no longer zero. In fact, on some occasions, the vorticity may approach infinity. Under this condition, the viscous effect, of course, becomes important.

Prompted by the occurrence of such unusual occasions, perhaps it should be suggested that the vorticity consideration on the jet boundary is not important and should not be taken into consideration in the establishment of the asymptotic profile since viscous mixing does occur along the free jet boundary in actual flows. Whether this change in approach would result in simpler analysis or simpler asymptotic profiles is yet to be examined.

4. CONCLUSIONS

From this study, it is recognized that a strong curved shock flow regime exists in the operation of the convergent-divergent nozzle. Although the precise manner of change-over between the Mach reflection and the present curved shock flow regimes has not been clearly defined, the pattern of the flow field associated with the occurrence of a strong curved shock is, nevertheless, established, and the gap of information on nozzles operating under these conditions is satisfactorily filled. The inviscid flow analysis of nozzle flow problems thus yields consistent flow patterns throughout the entire range of the pressure ratio.

In the study of the flow field within this flow regime, it is immediately recognized that an integral constraining relationship exists at the asymptotic state which points out the inadequacy of the indirect approach to the problem. Instead of asserting that the flow field is produced as a result of the upstream shock, it may be interpreted that the prevailing ambient and the asymptotic conditions forced the appearance of the shock with a specific geometry. This is, of course, typical for all elliptic types of flow problems.

The suggested method of solution to these problems relies on the selection of the asymptotic profile. It is not known whether there exist other approaches or methods which are equally effective in dealing with these problems.

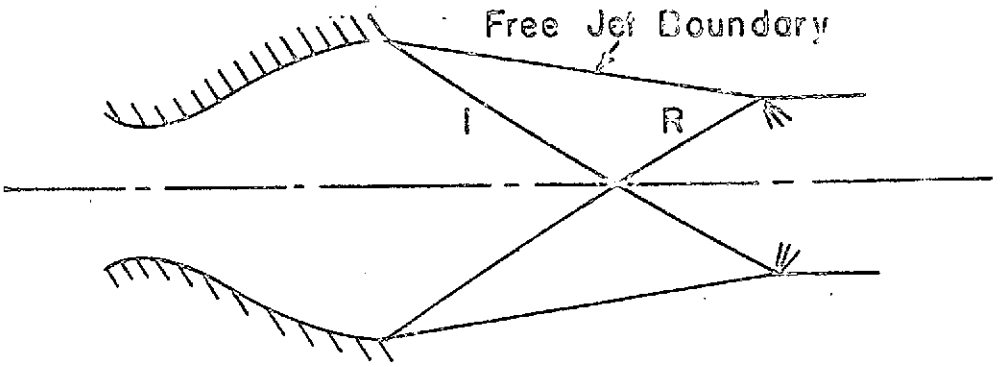

Figure 1a Regular Reflection produced from Two-Dimensional Overexpanded Nozzle Flow

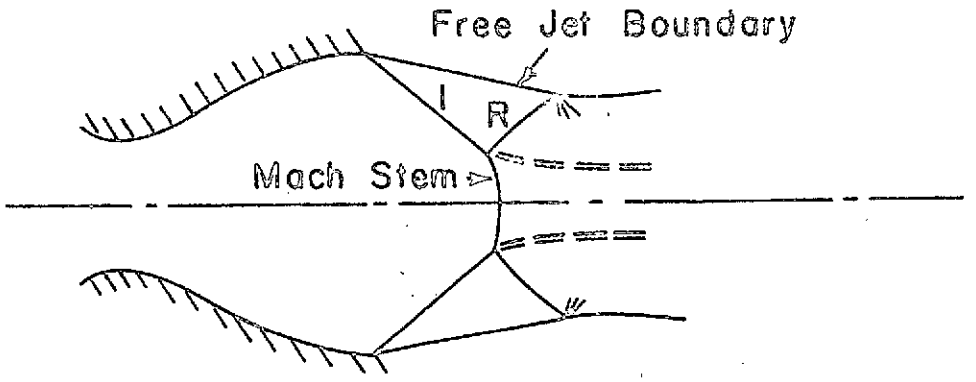

Figure 1b Mach Reflection produced from Two-Dimensional Overexpanded Nozzle Flow

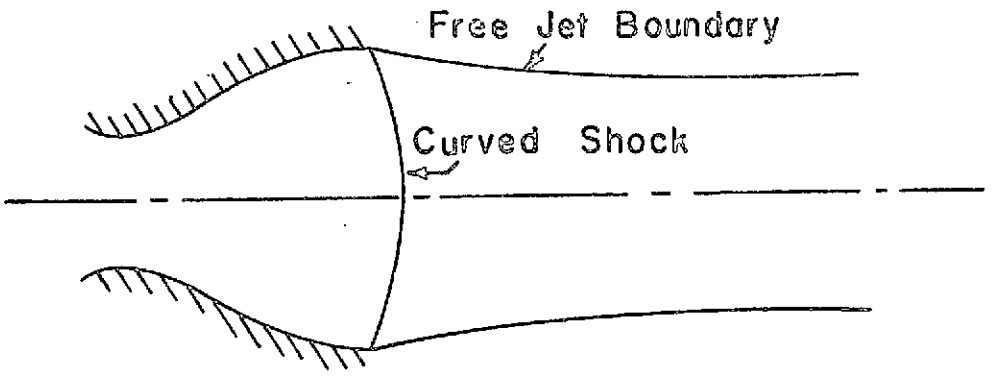

Figure 1c Curved Shock produced from Two-Dimensional Overexpanded Nozzle Flow

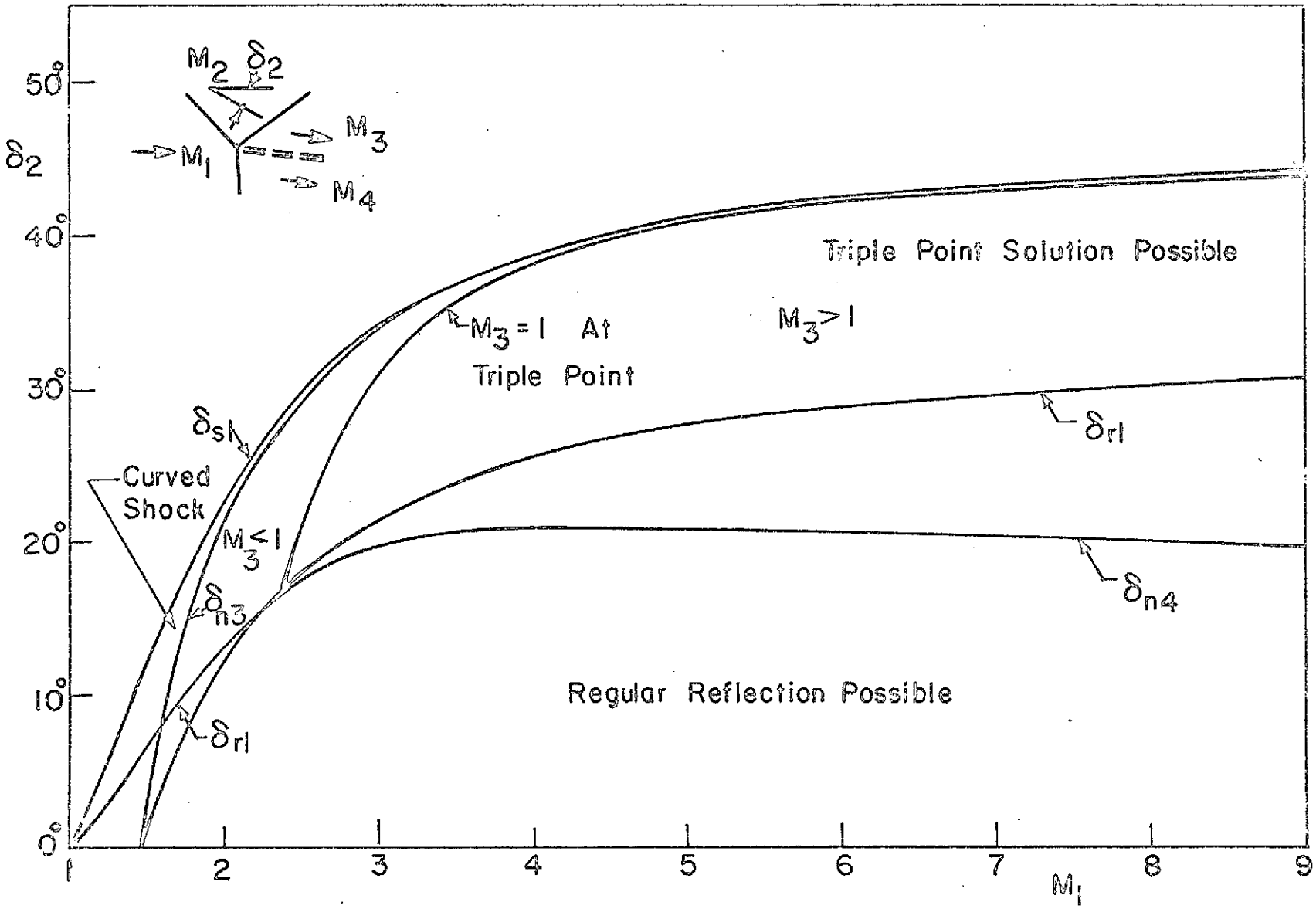

Figure 2 Regions of Regular, Mach Reflection, and Curved Shock, δ_2 vs M_1 [4]

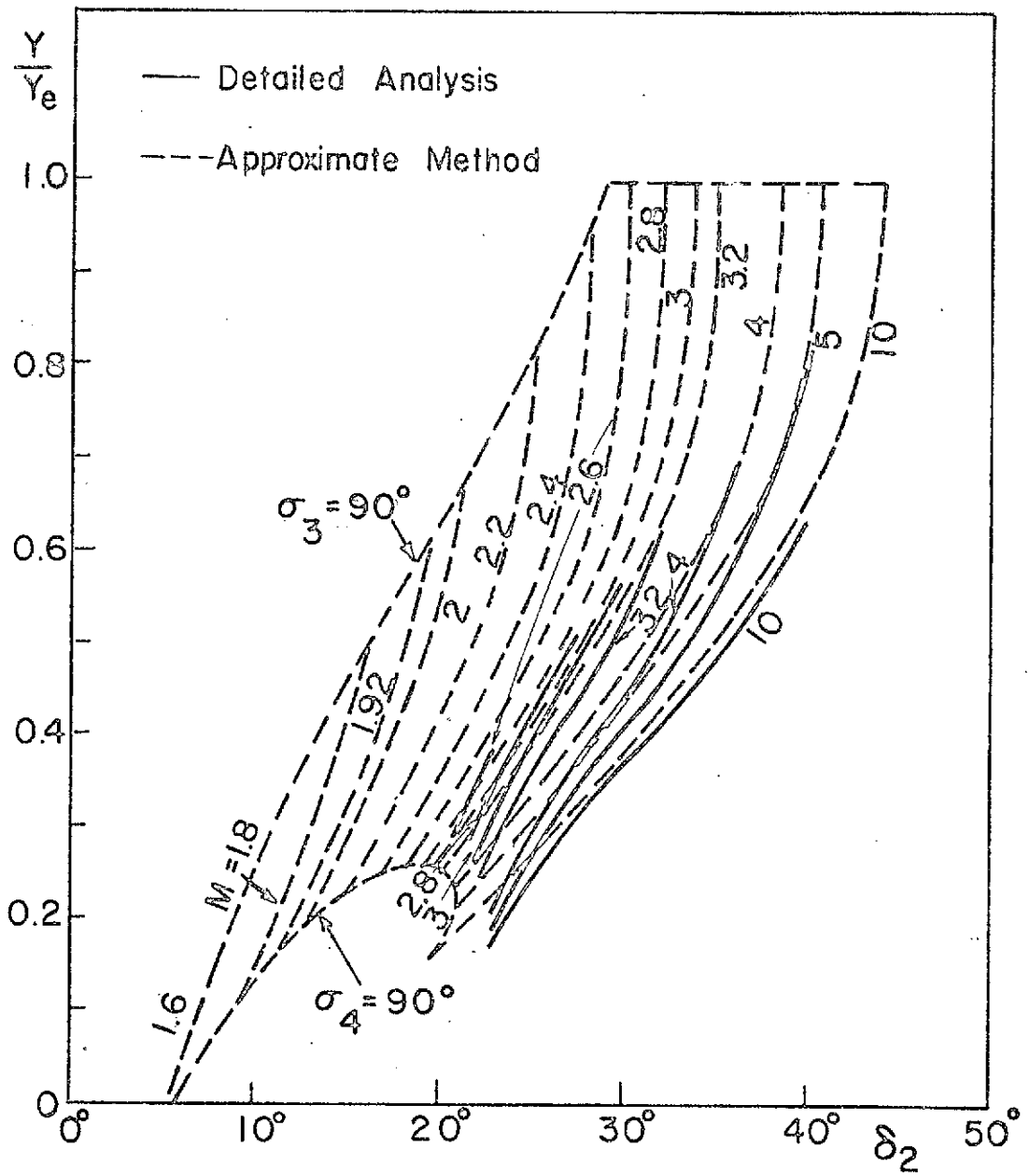

Figure 3 Mach Stem Height y/y_e for δ_2 for Two-Dimensional Overexpanded Nozzle Flow [4]

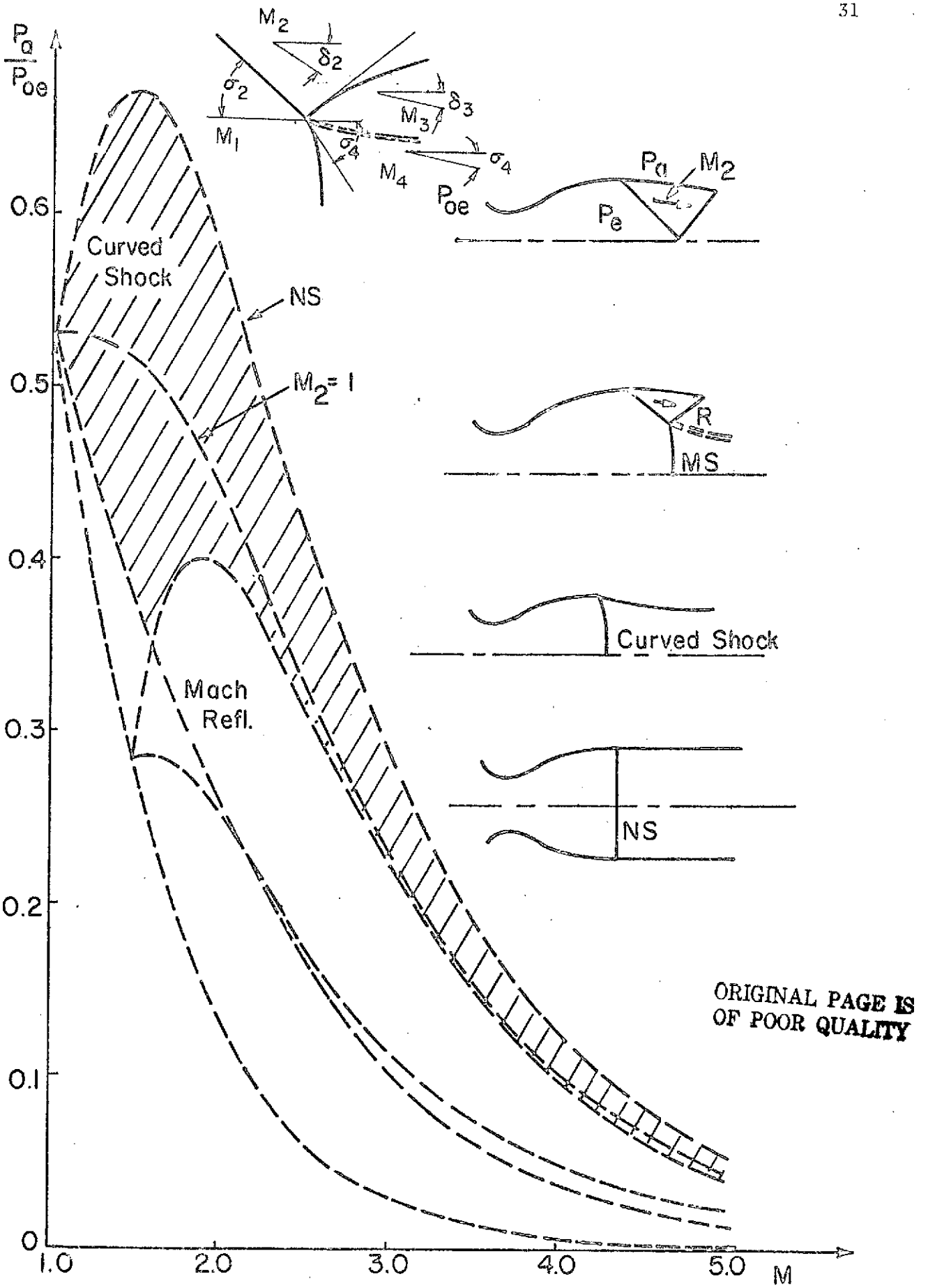

ORIGINAL PAGE IS
OF POOR QUALITY

Figure 4 Regions of Regular, Mach Reflection, and Curved Shock, p_a/p_{oe} vs M [4]

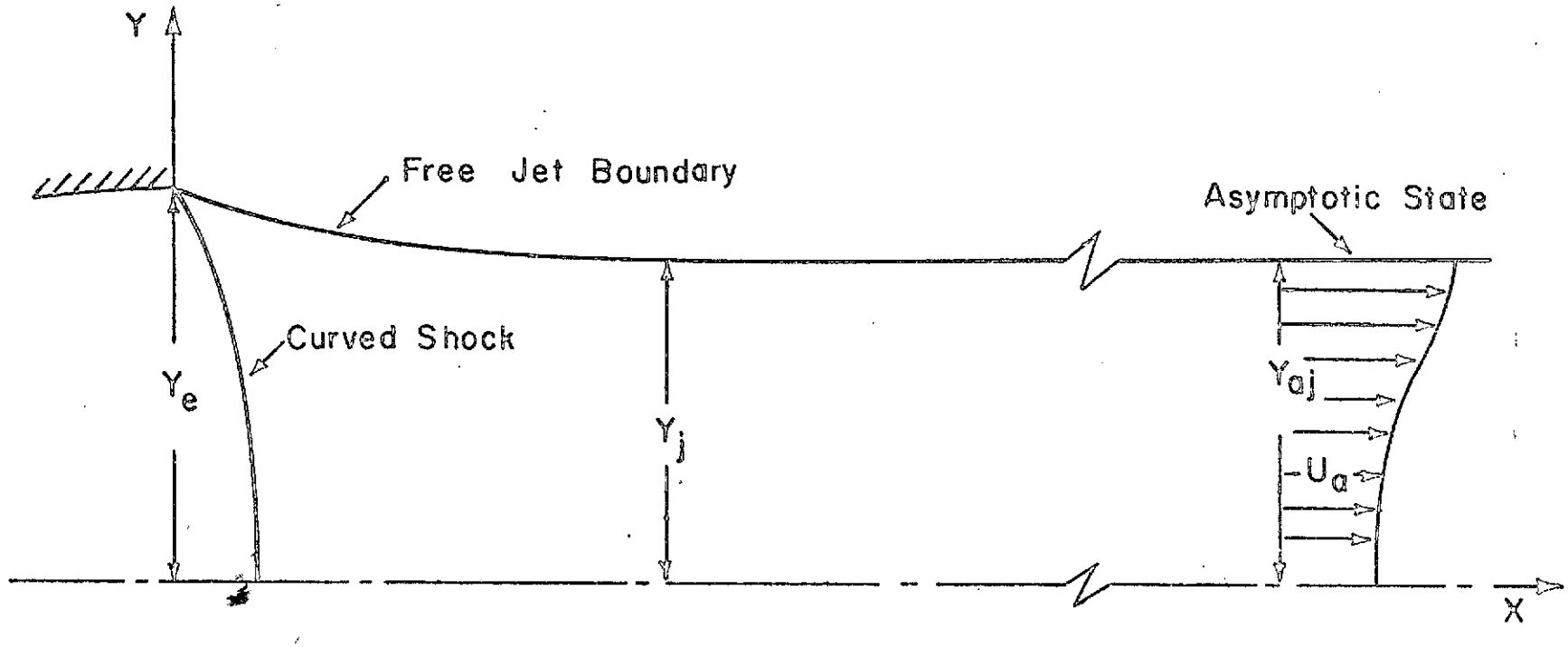

Figure 5 Schematic Diagram of Configuration Considered

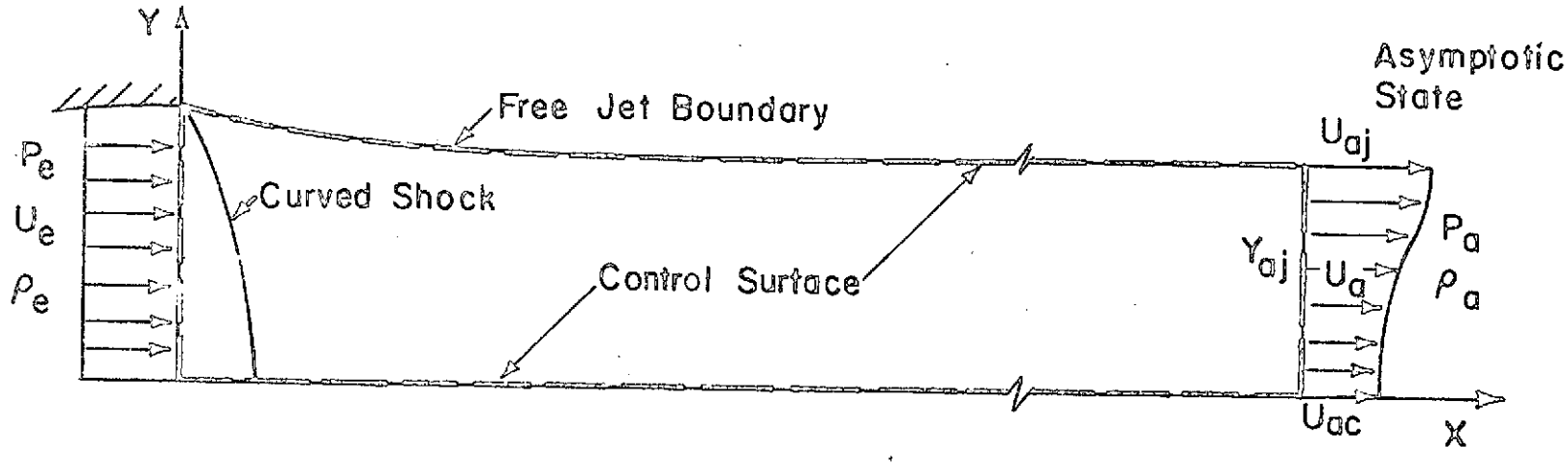

Figure 6a Control Volume for Calculating the Asymptotic Velocity Profile

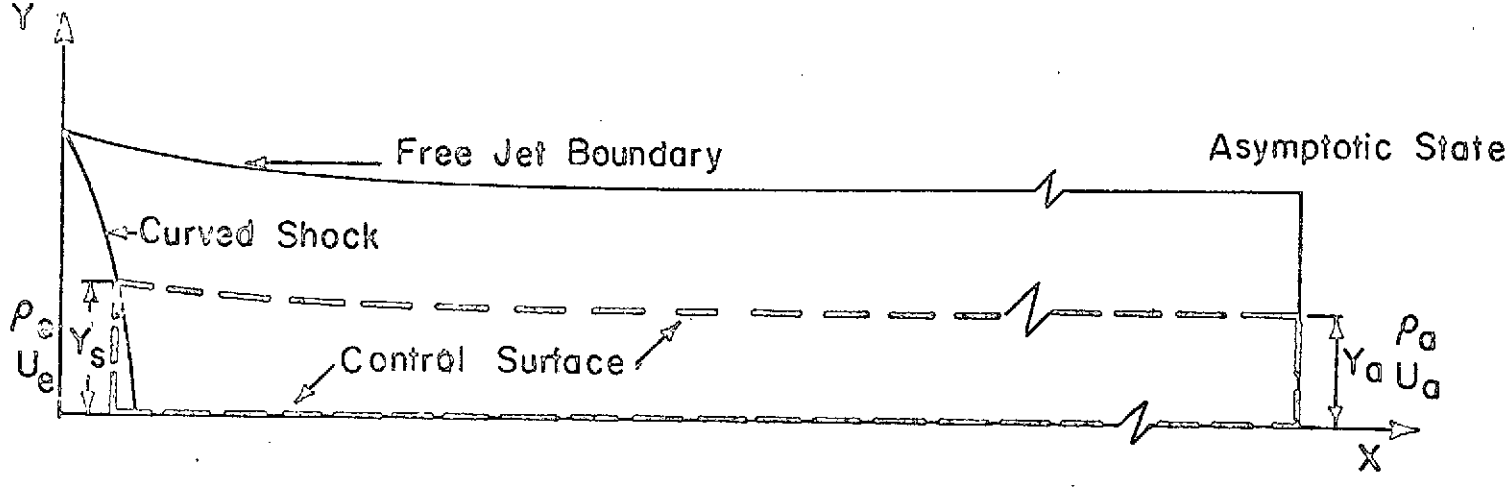

Figure 6b Control Volume for Calculating Shock Height y_s

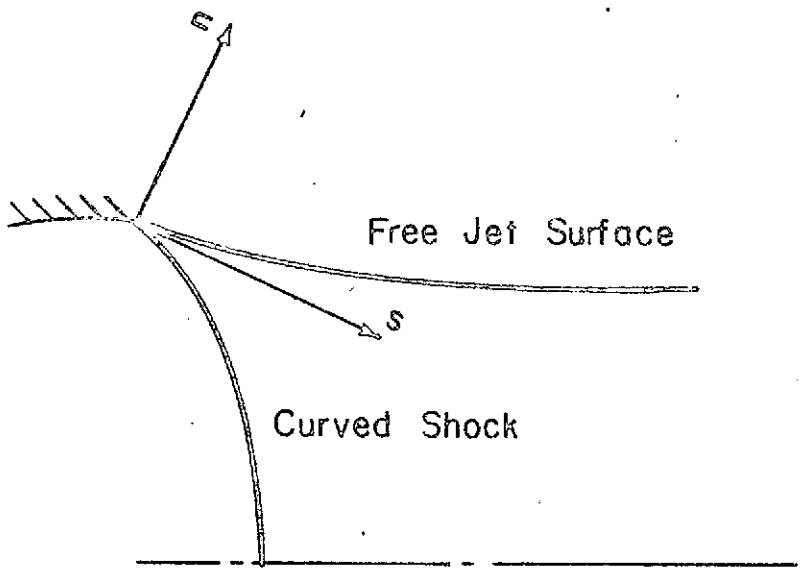

Figure 7 Shock Configuration at Corner of Nozzle

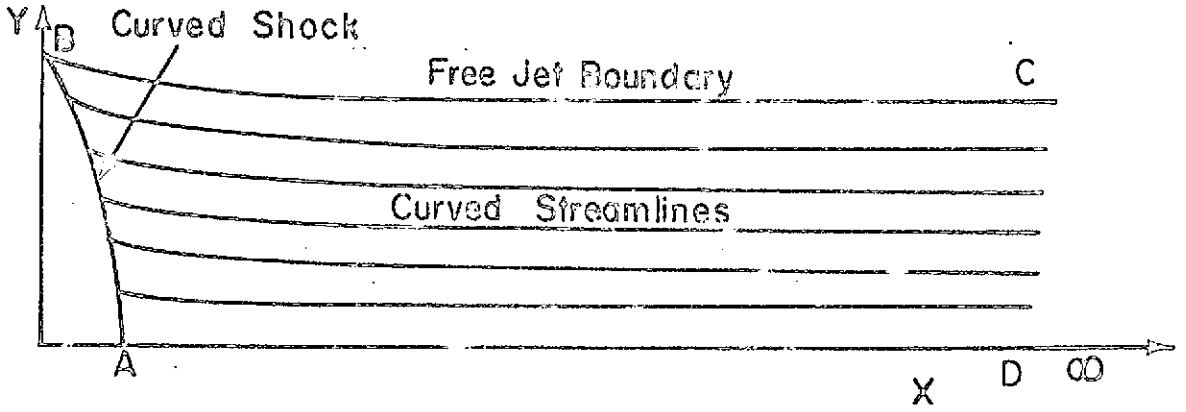

(a) Physical Plane

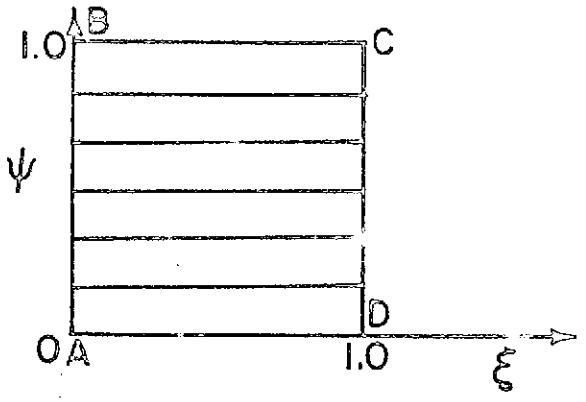

(b) Computational Plane

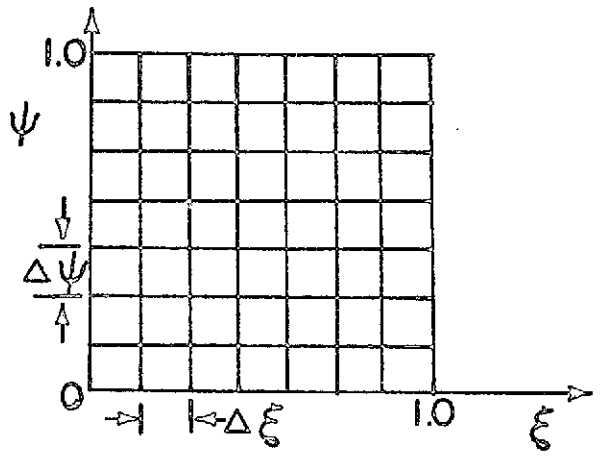

(c) Computational Plane

Figure 8 Coordinate Transformation

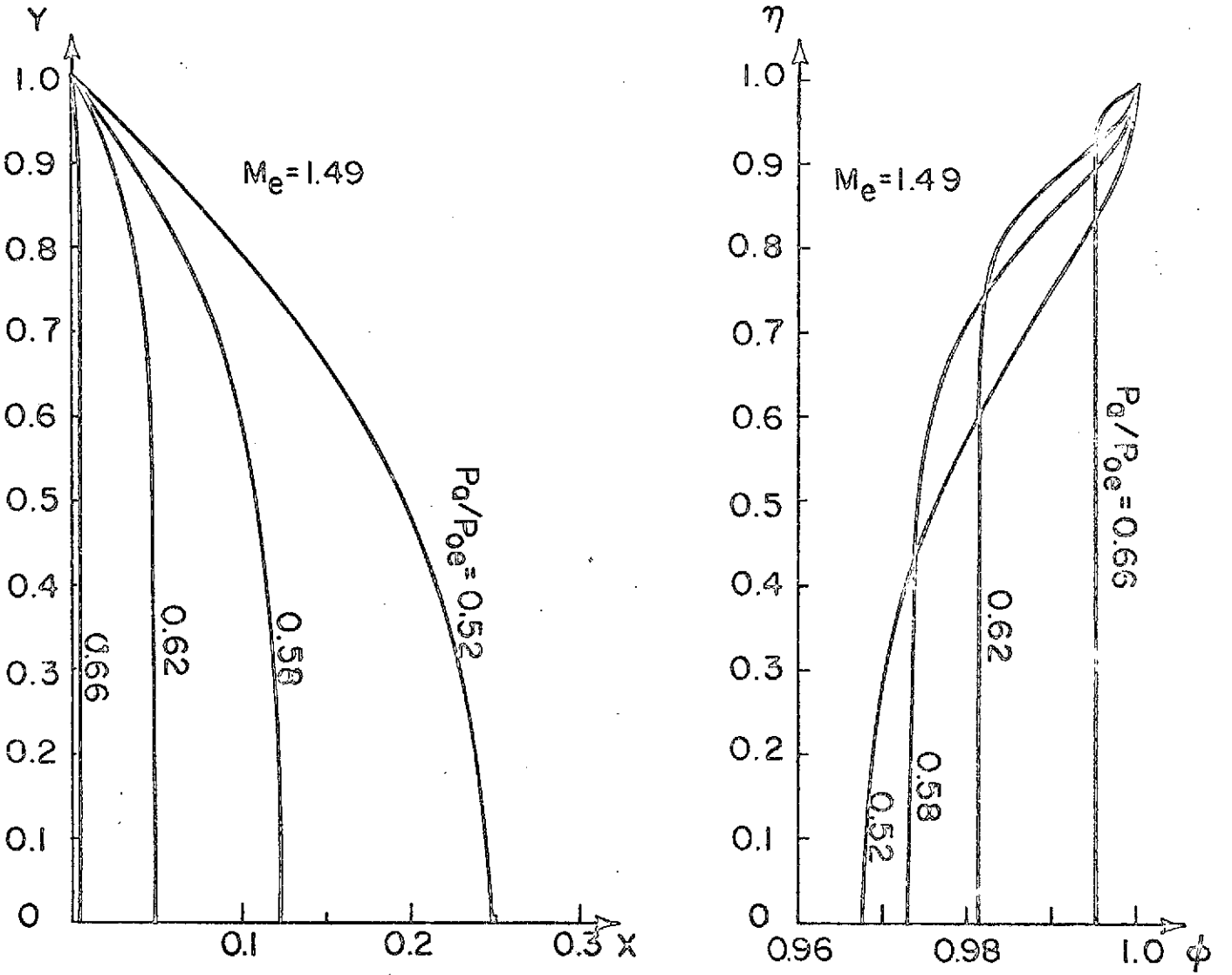

Figure 9a Curved Shock and Asymptotic Velocity Profiles for M_e = 1.49

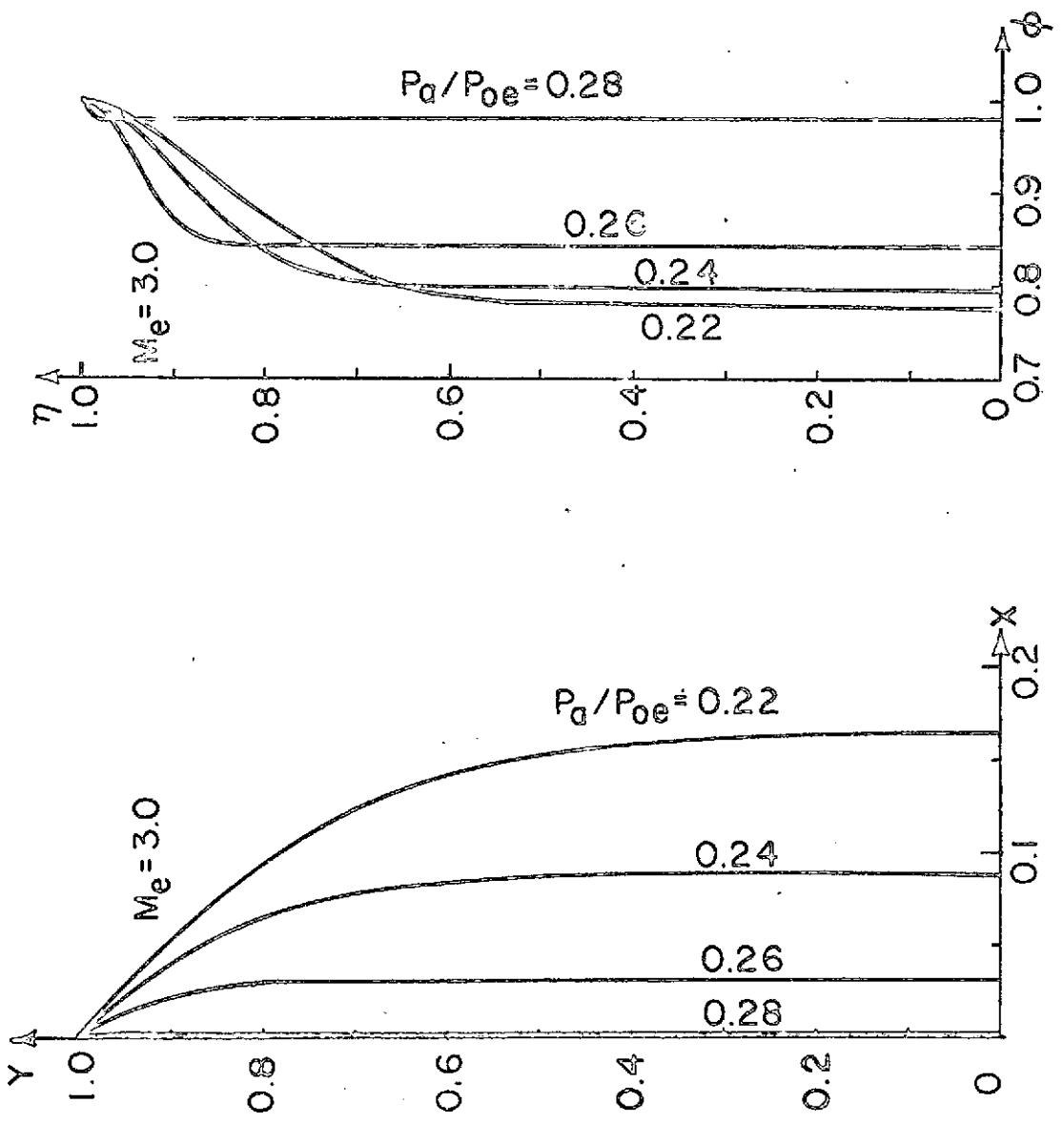

Figure 9b Curved Shock and Asymptotic Velocity Profiles for M_e = 3.0

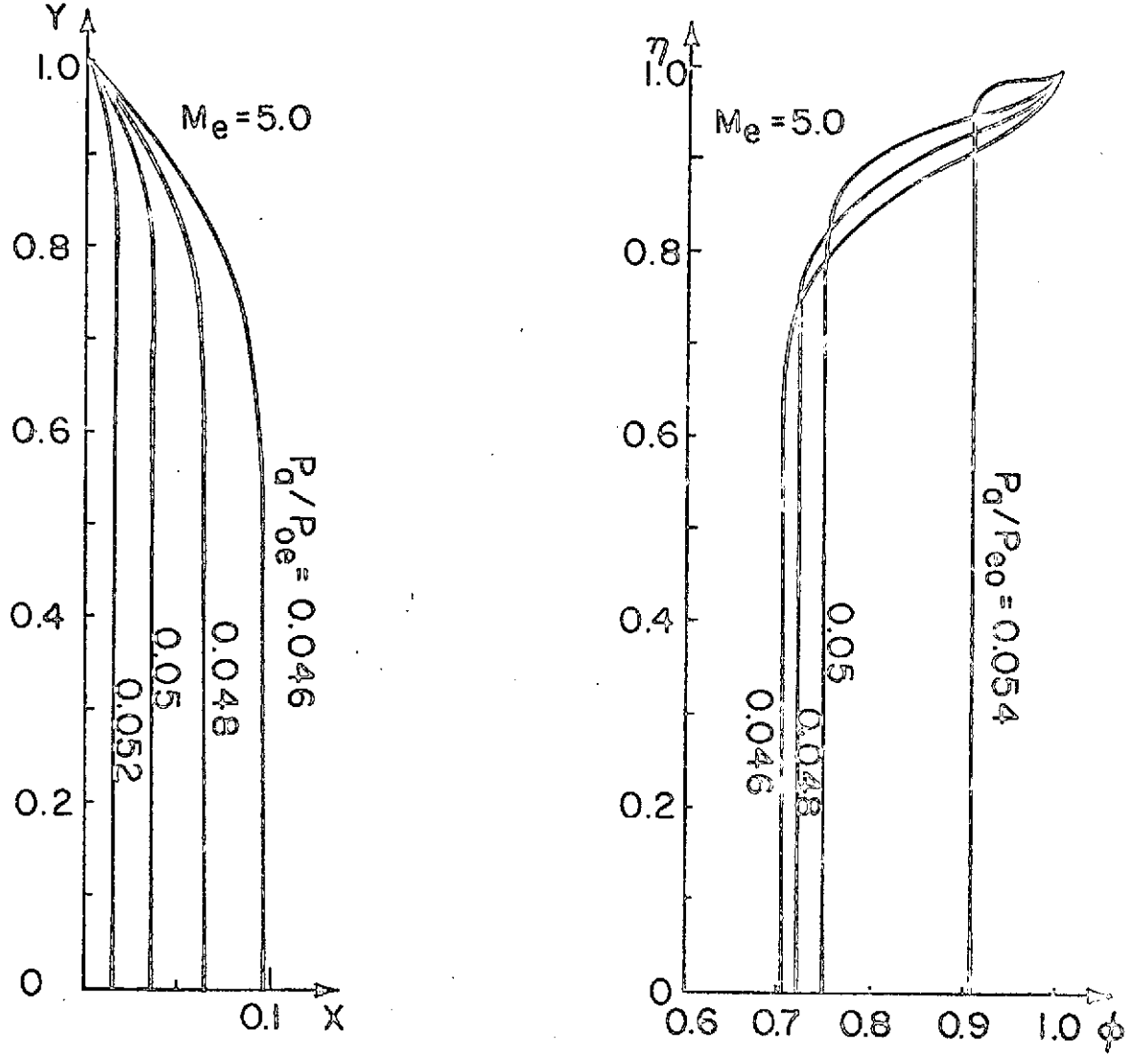

Curved Shock Profile

Asymptotic Velocity Profile

Figure 9c Curved Shock and Asymptotic Velocity Profiles for $M_e = 5.0$

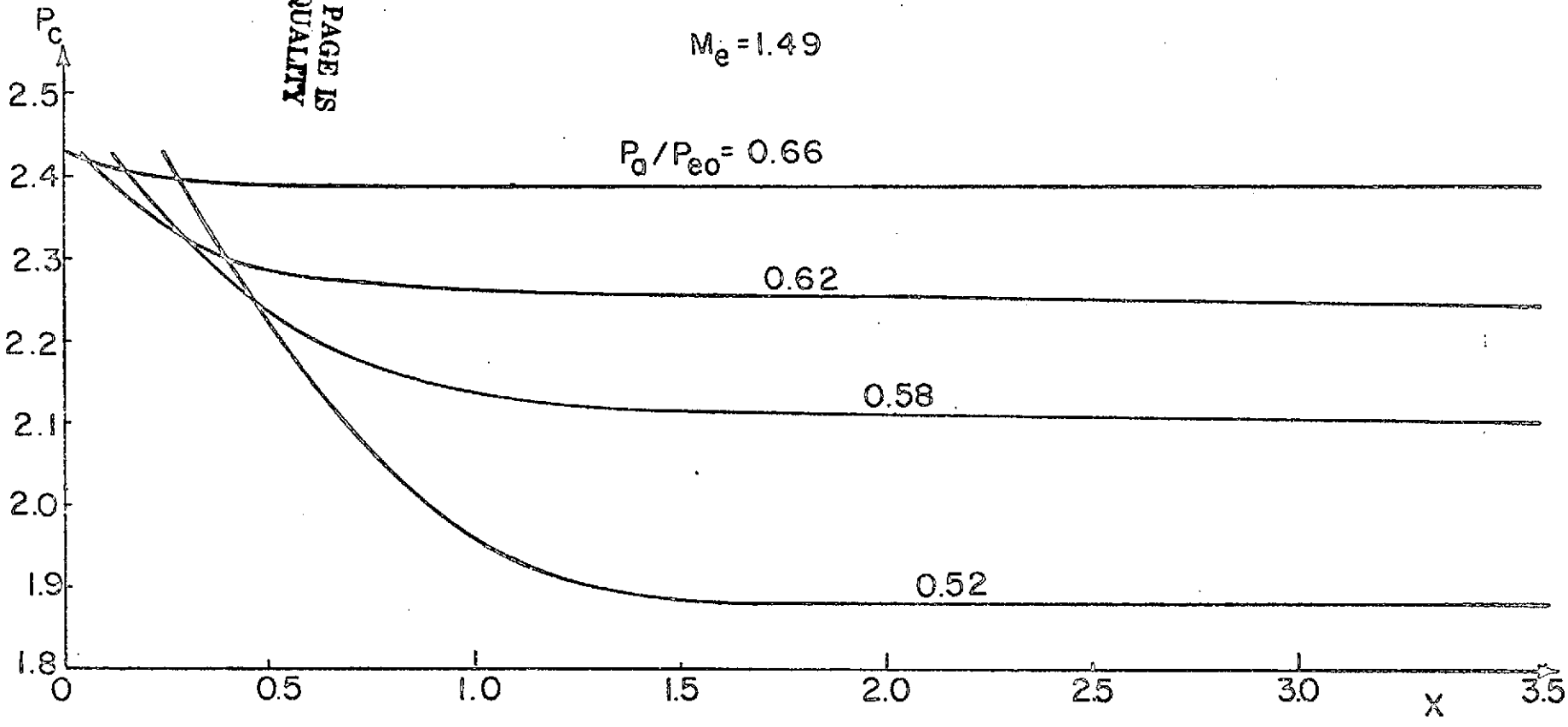

Figure 10a Variation of Centerline Pressure for $M_e = 1.49$

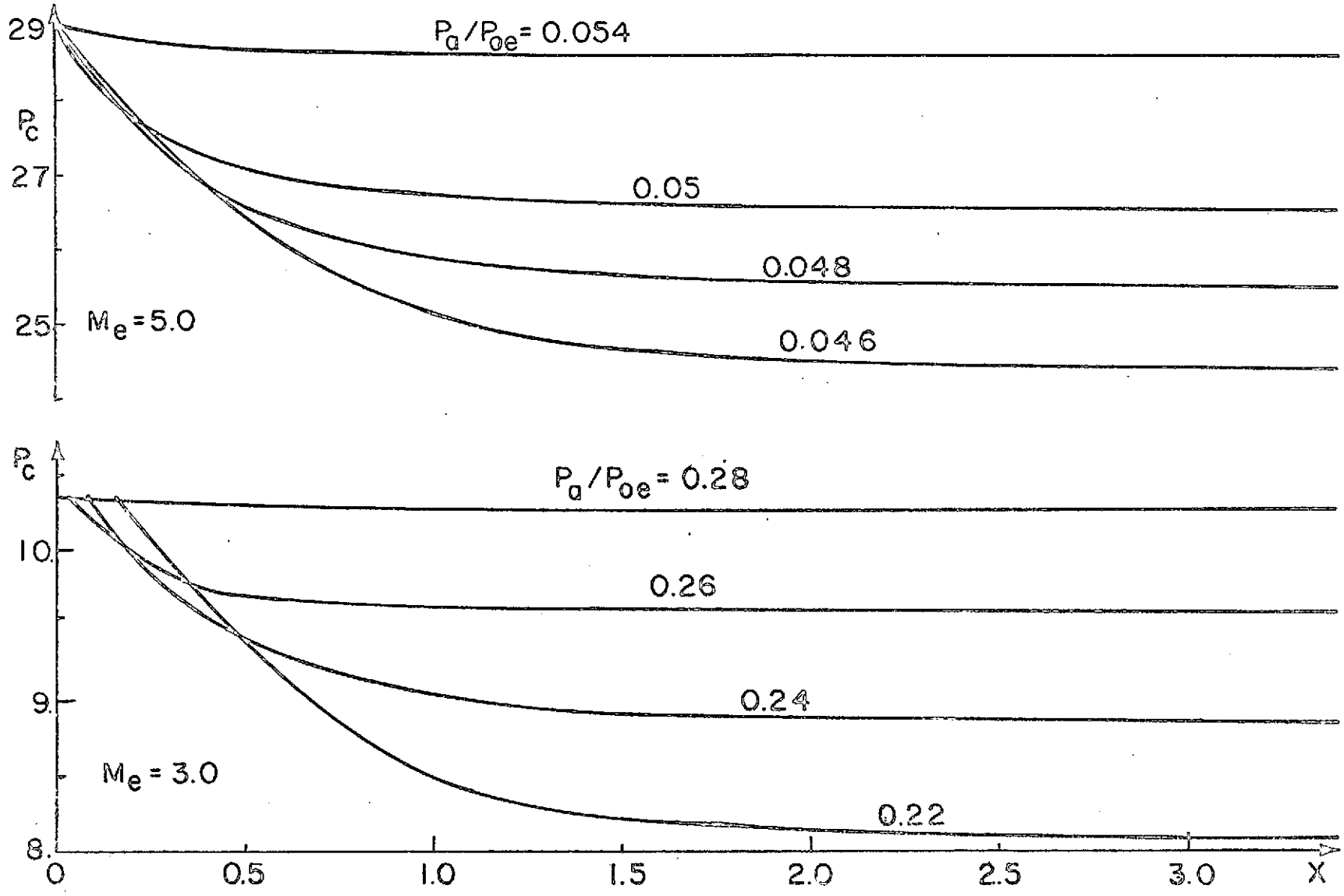

Figure 10b Variation of Centerline Pressure for M_e = 3.0 and 5.0

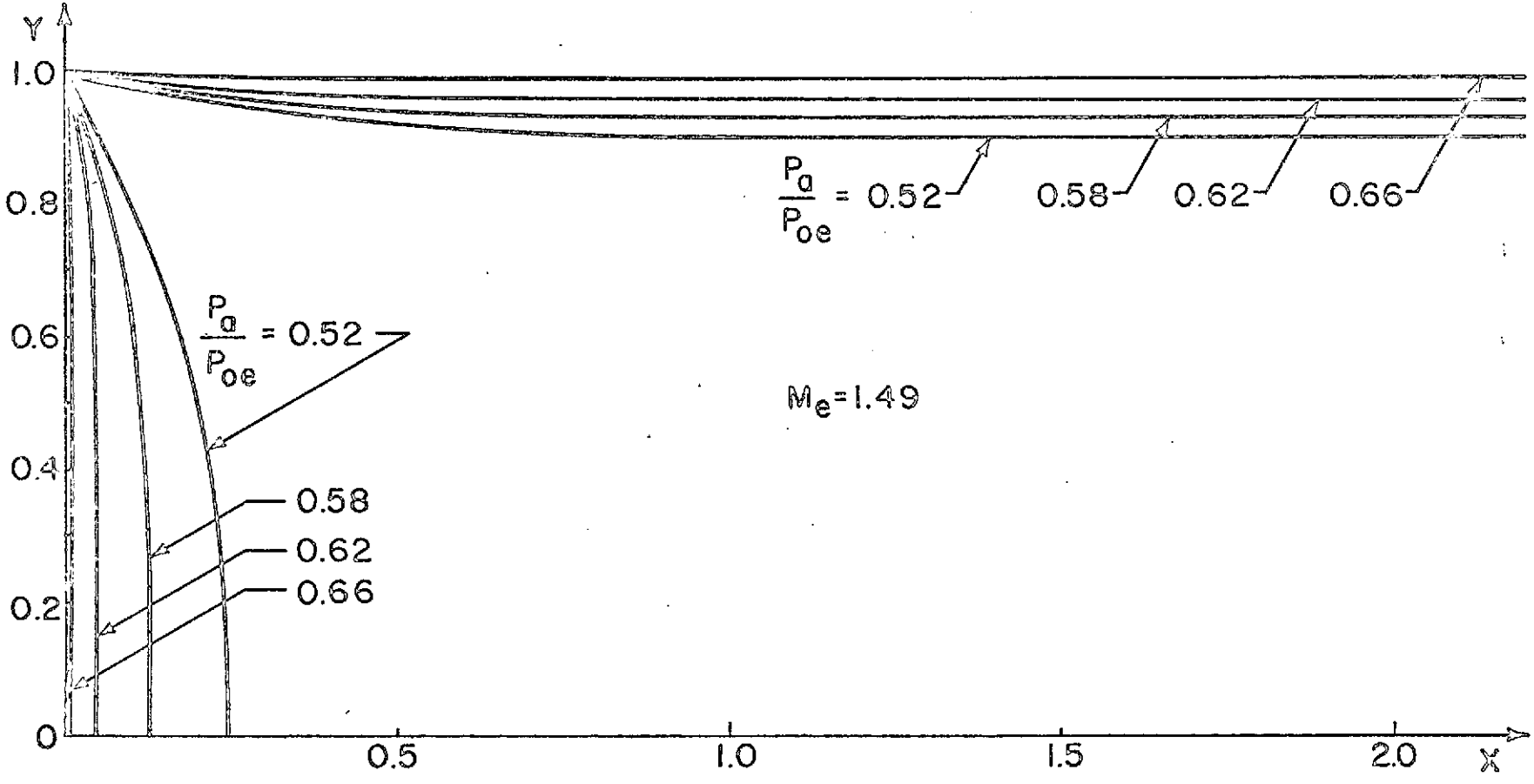

Figure 11a Curved Shock and Free Jet Boundary Profiles for M_e = 1.49

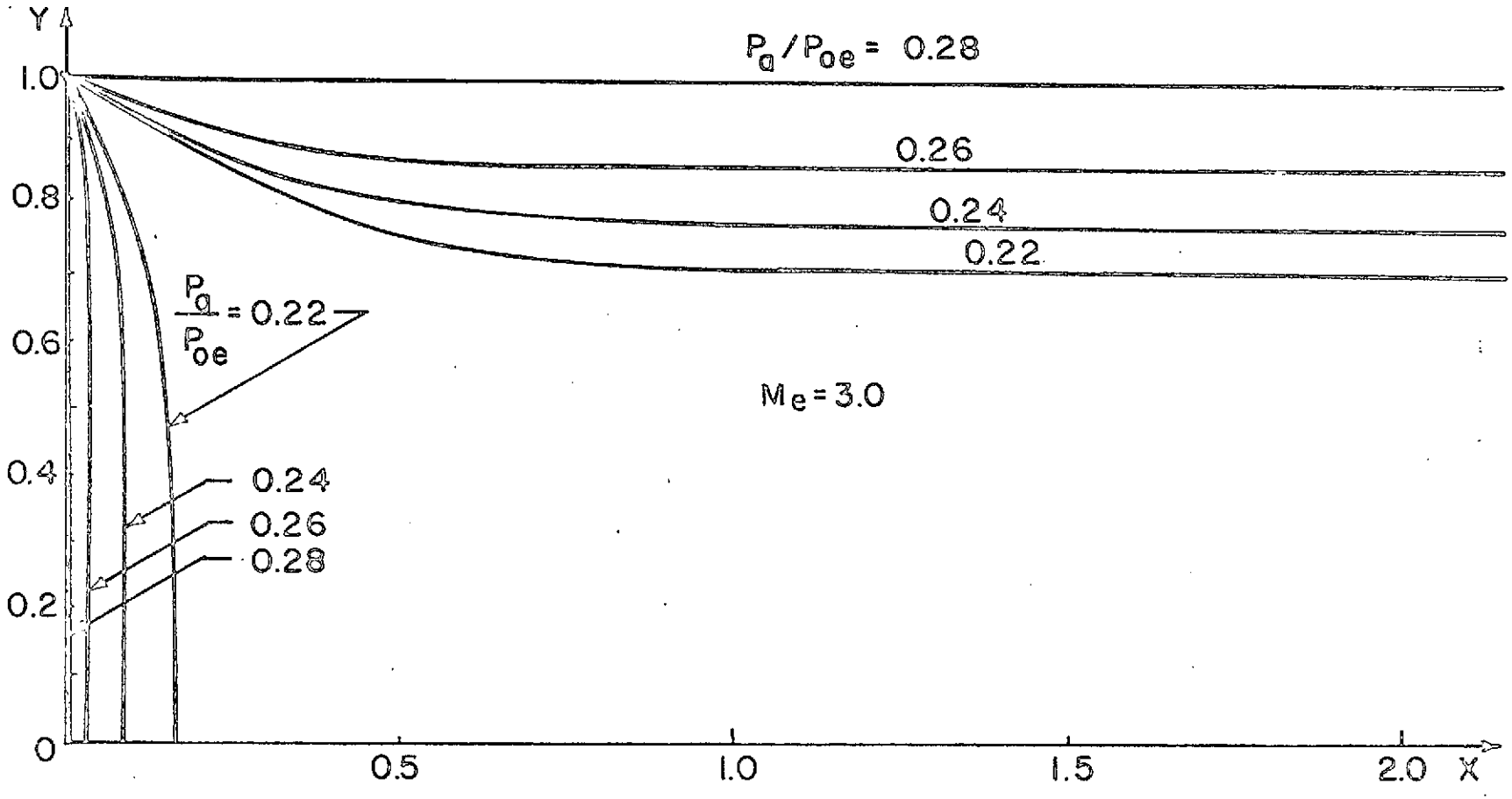

Figure 11b Curved Shock and Free Jet Boundary Profiles for M_e = 3.0

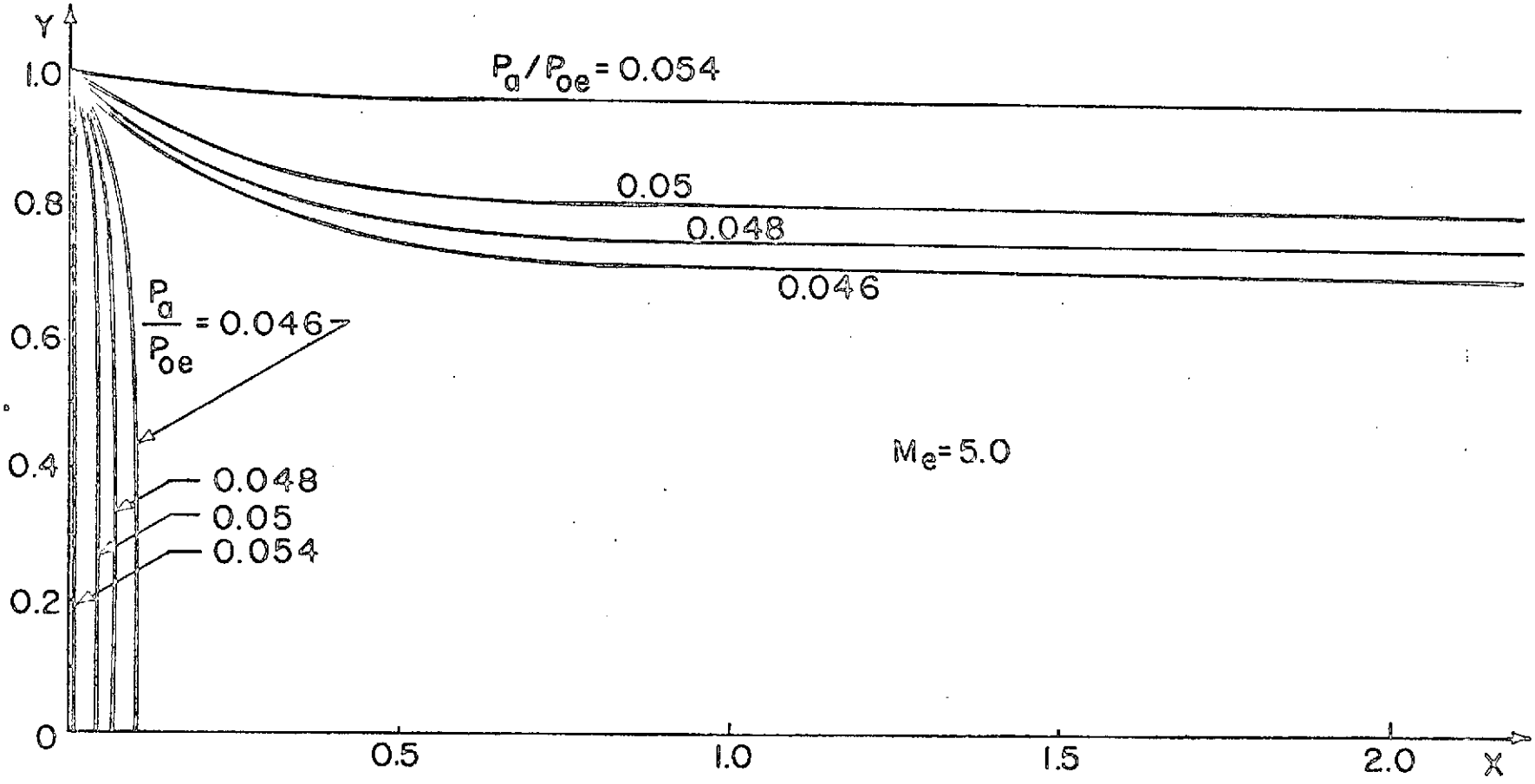

Figure 11c Curved Shock and Free Jet Boundary Profiles for M_e = 5.0

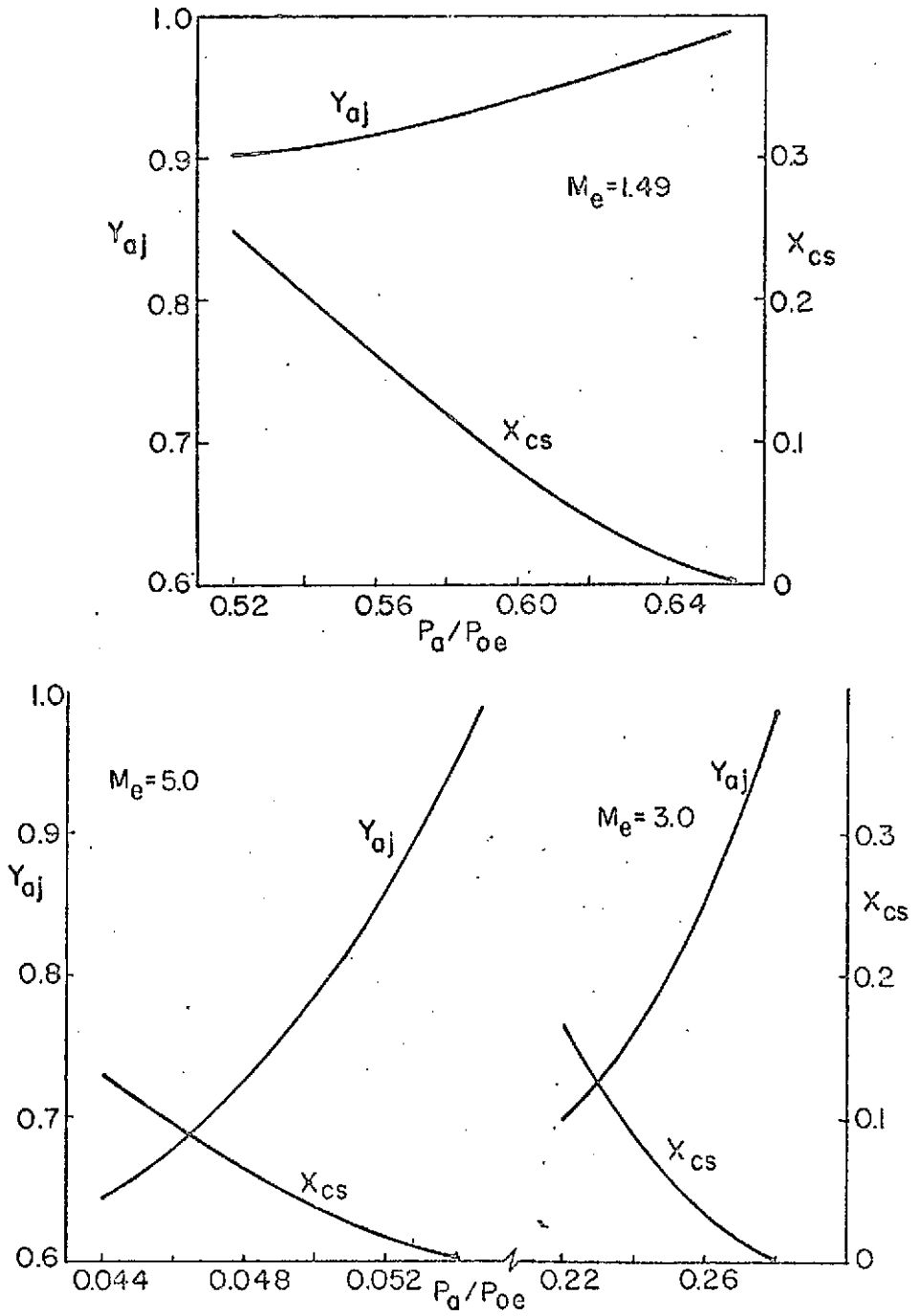

Figure 12 Variation of Asymptotic Free Jet Height y_{aj} and Shock Standout Distance x_{cs} with Respect to Pressure Ratio p_a/p_{oe} at M = 1.49, 3.0, and 5.0

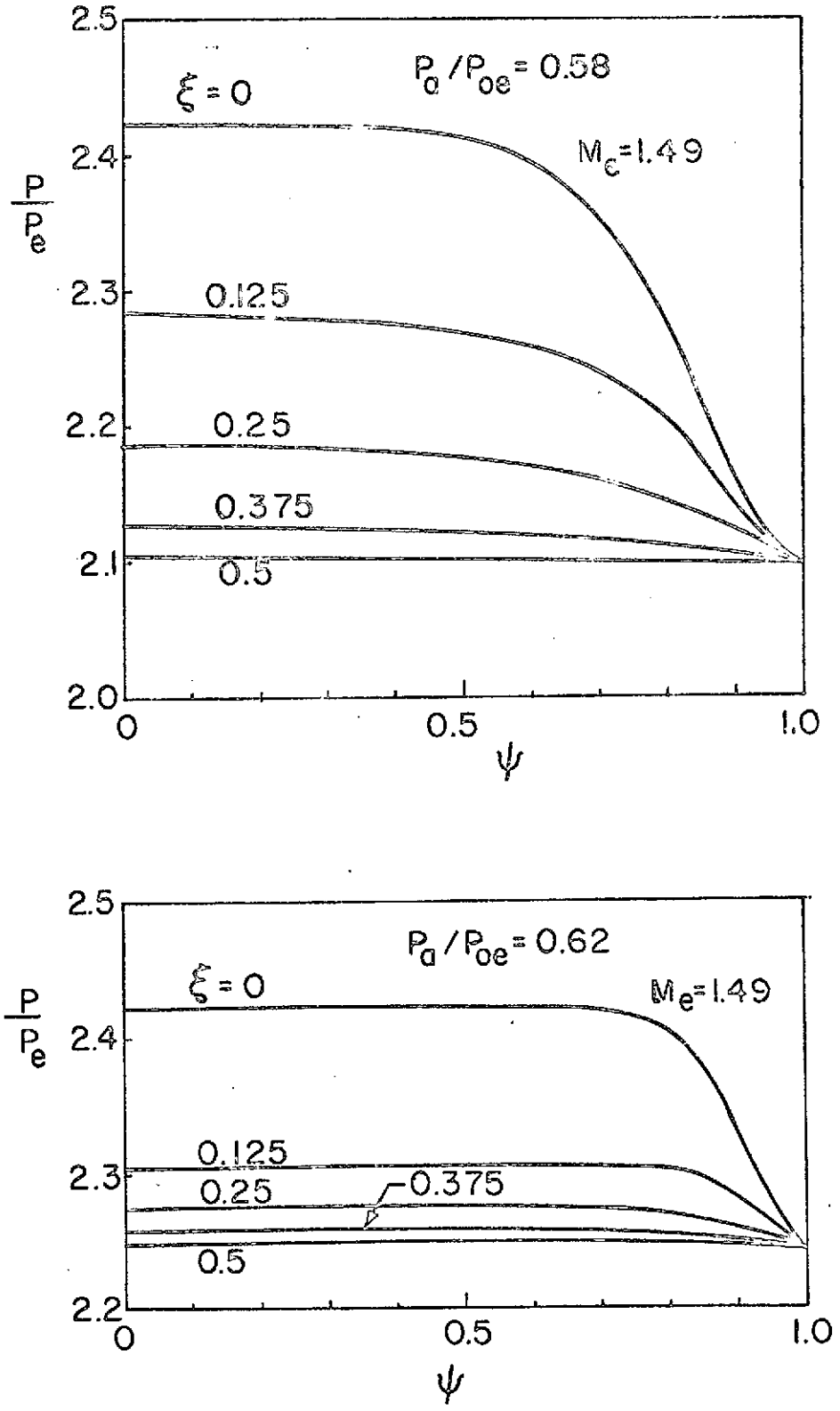

Figure 13a Pressure p/p_e Distribution for M_e = 1.49

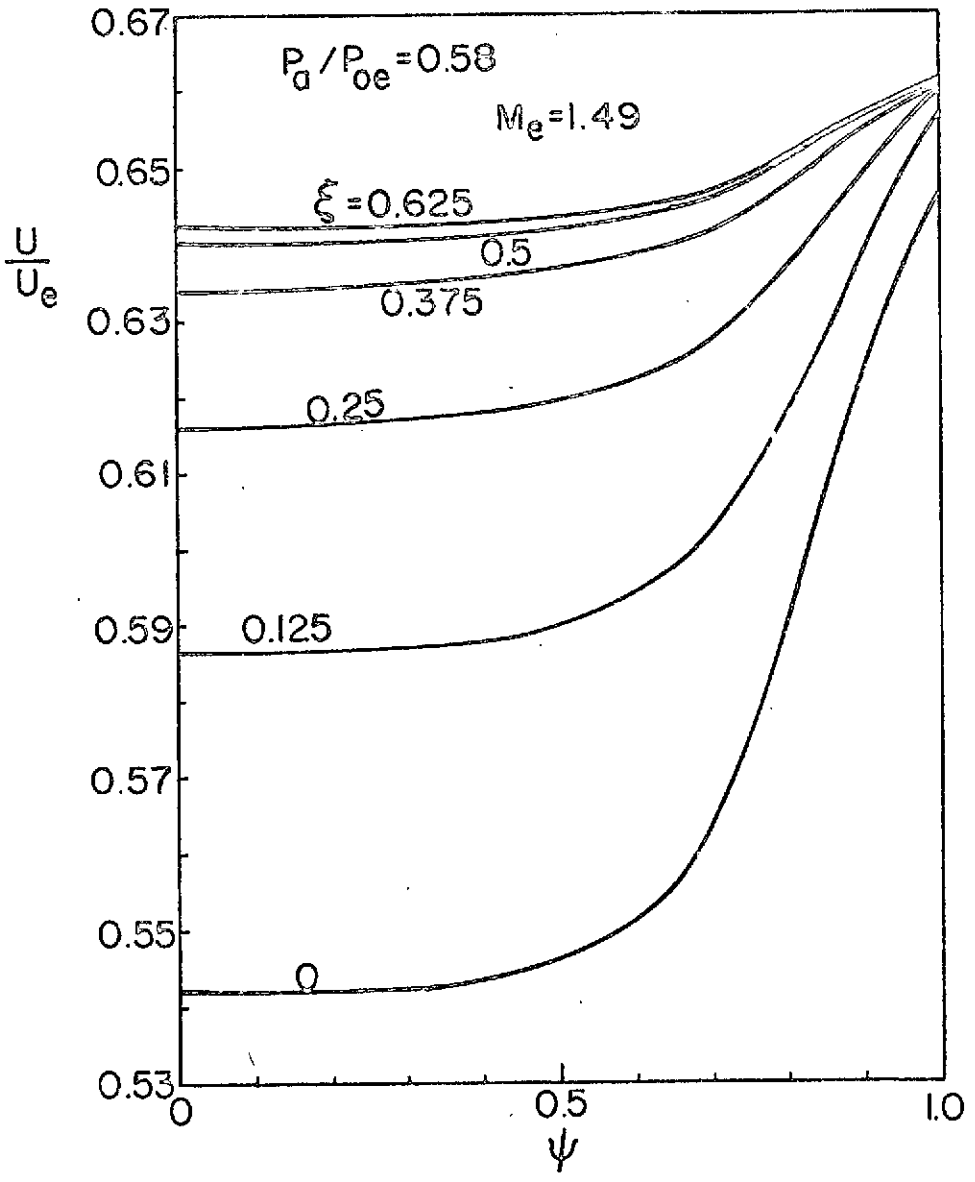

Figure 13b Velocity u Distribution for M_e = 1.49

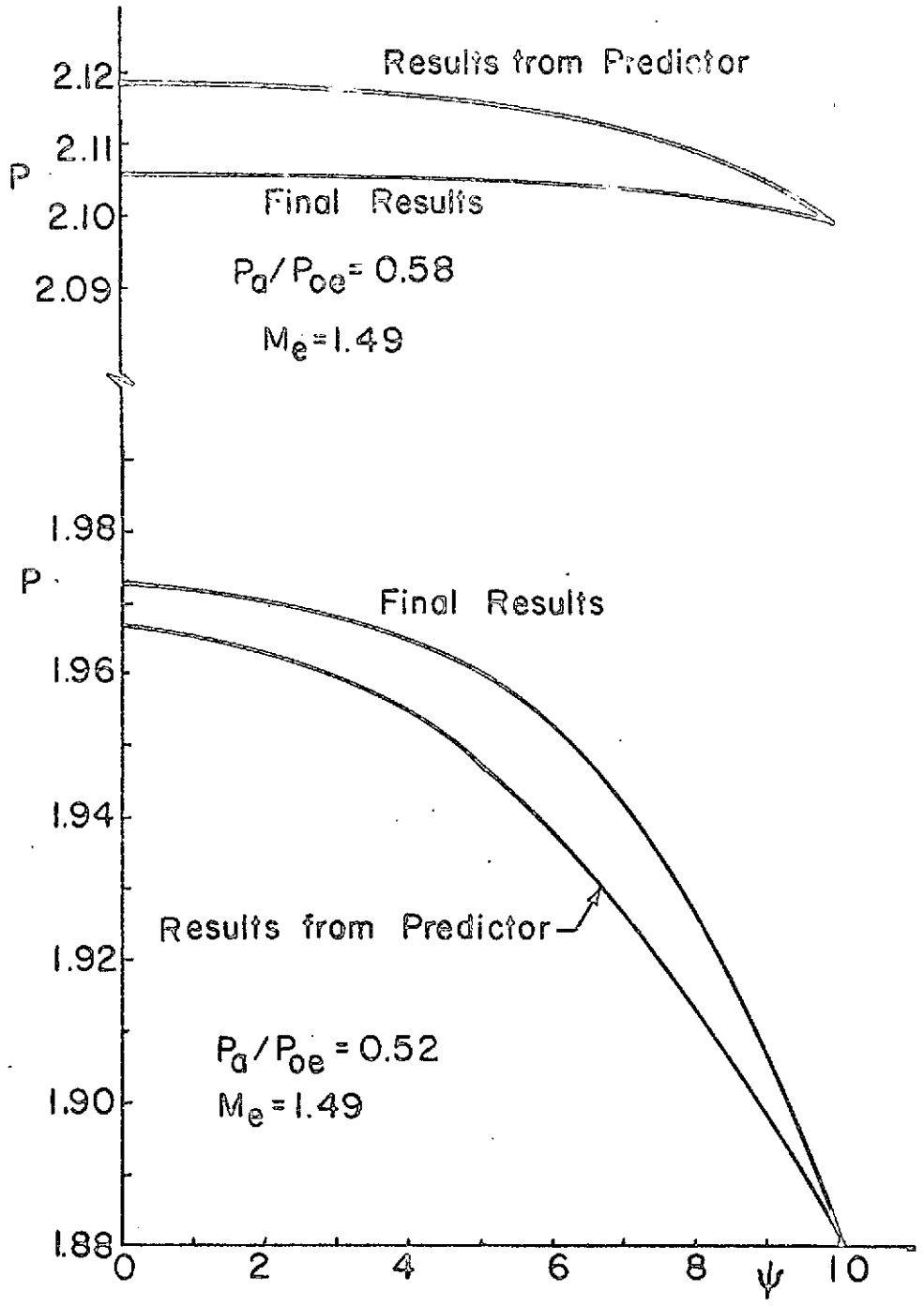

Figure 14 Results of Pressure Distribution along ξ = 0.5 from Predictor and Final Calculations for M_e = 1.49

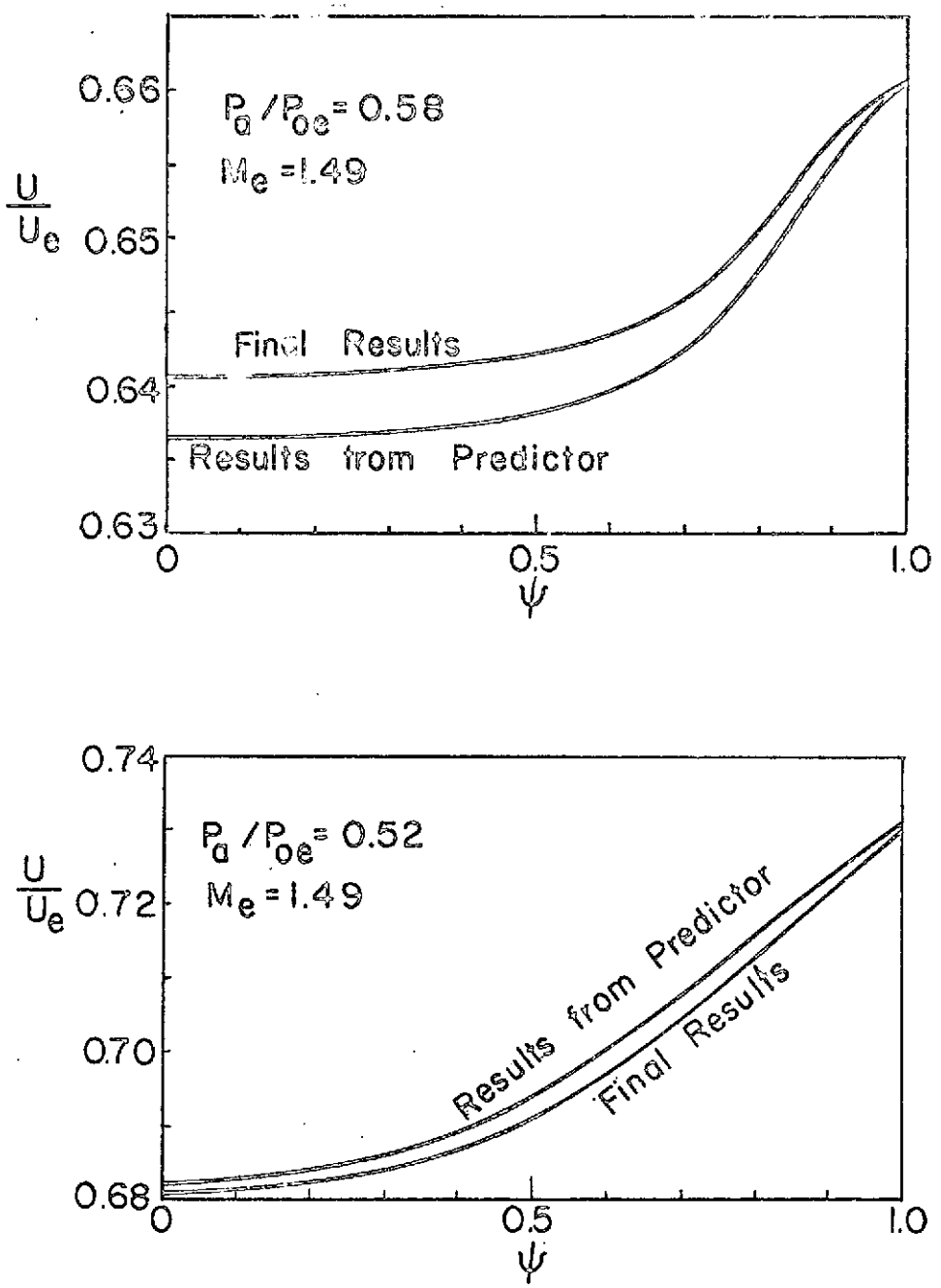

Figure 15 Results of Velocity u Distribution along ξ = 0.5 from Predictor and Final Calculations for M_e = 1.49

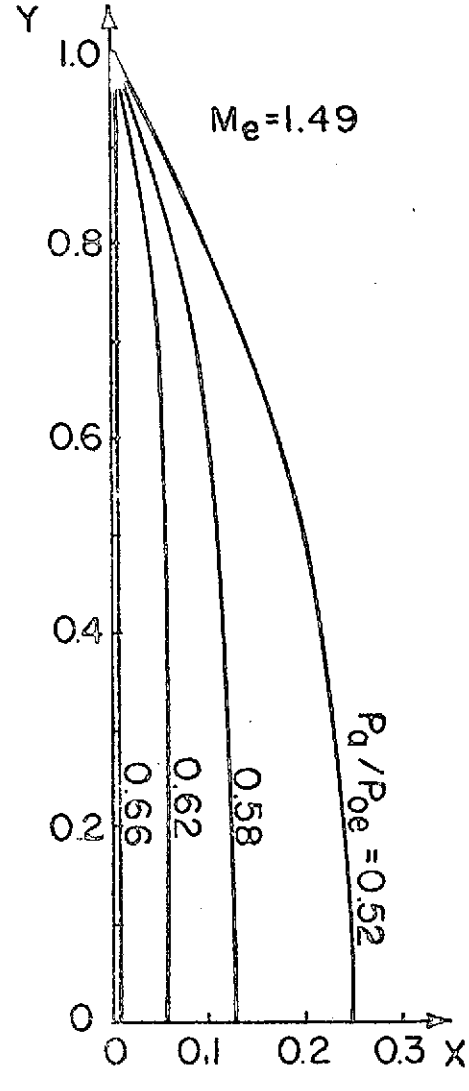

Curved Shock Profile

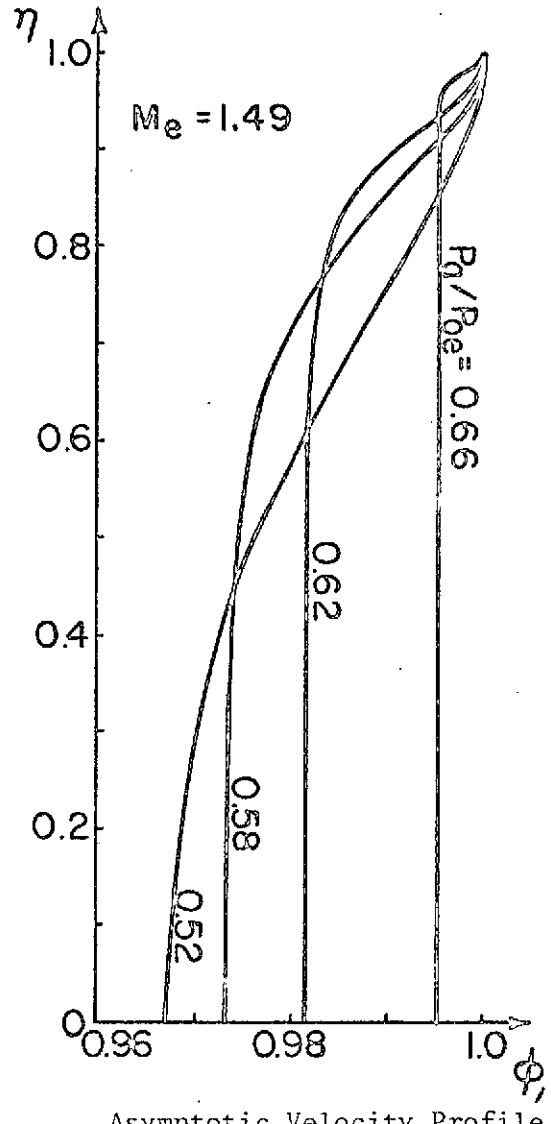

Asymptotic Velocity Profile

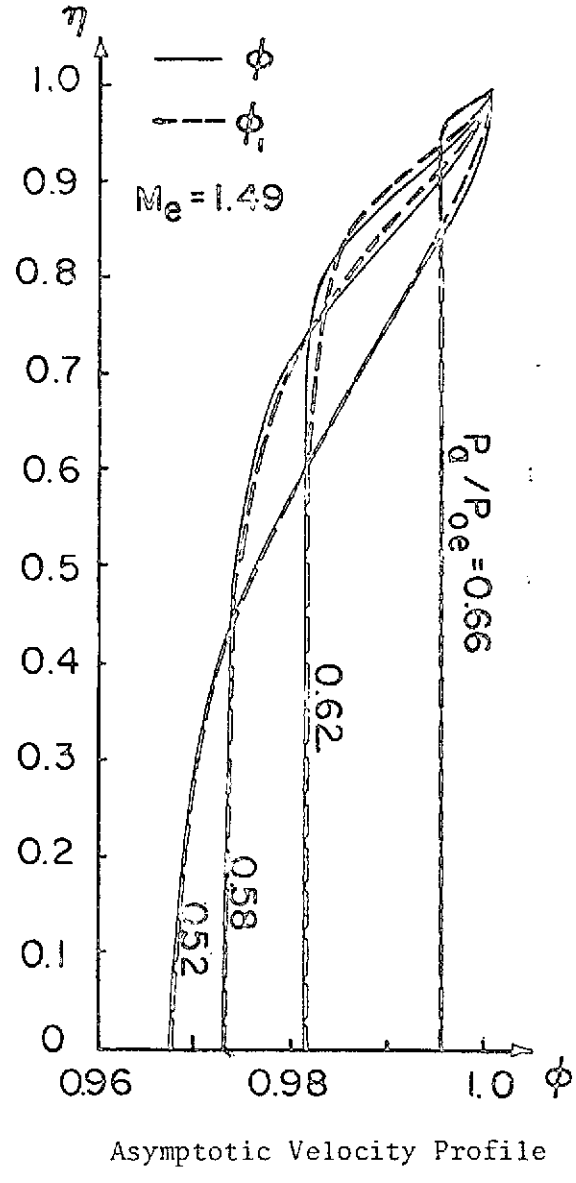

Asymptotic Velocity Profile

Figure 16 Curved Shock and Asymptotic Velocity Profiles for M_e = 1.49 and ϕ_1 = A + B tanh [C(1 - η^2)] + D tanh [C(1 - η^4)]

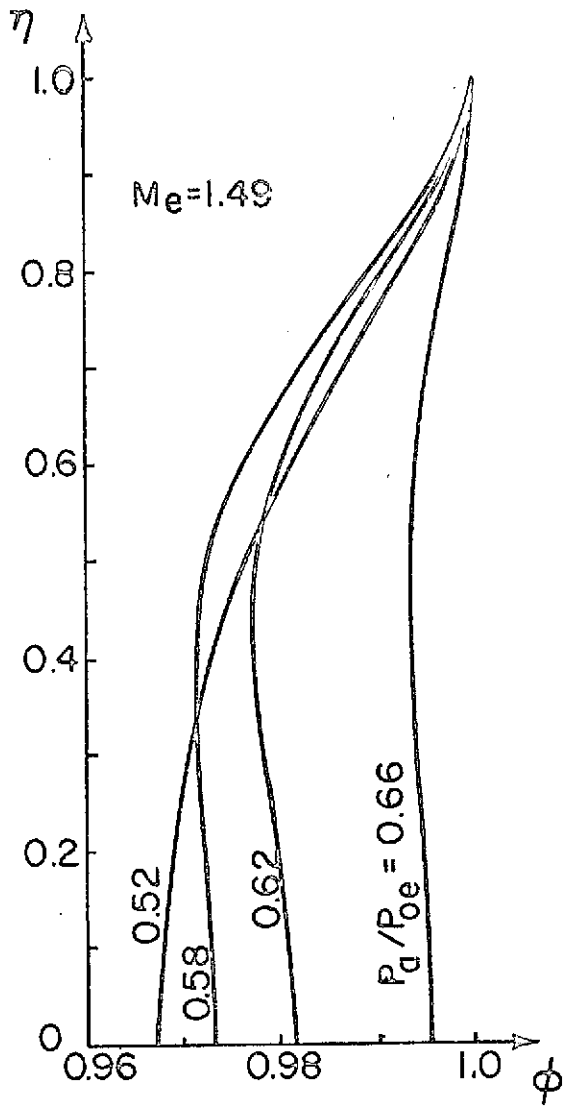

Figure 17 Asymptotic Velocity Proile for M_e = 1.49 and $\phi_2 = A + B\,\eta^2 + C\,\eta^4 + D\,\eta^6$

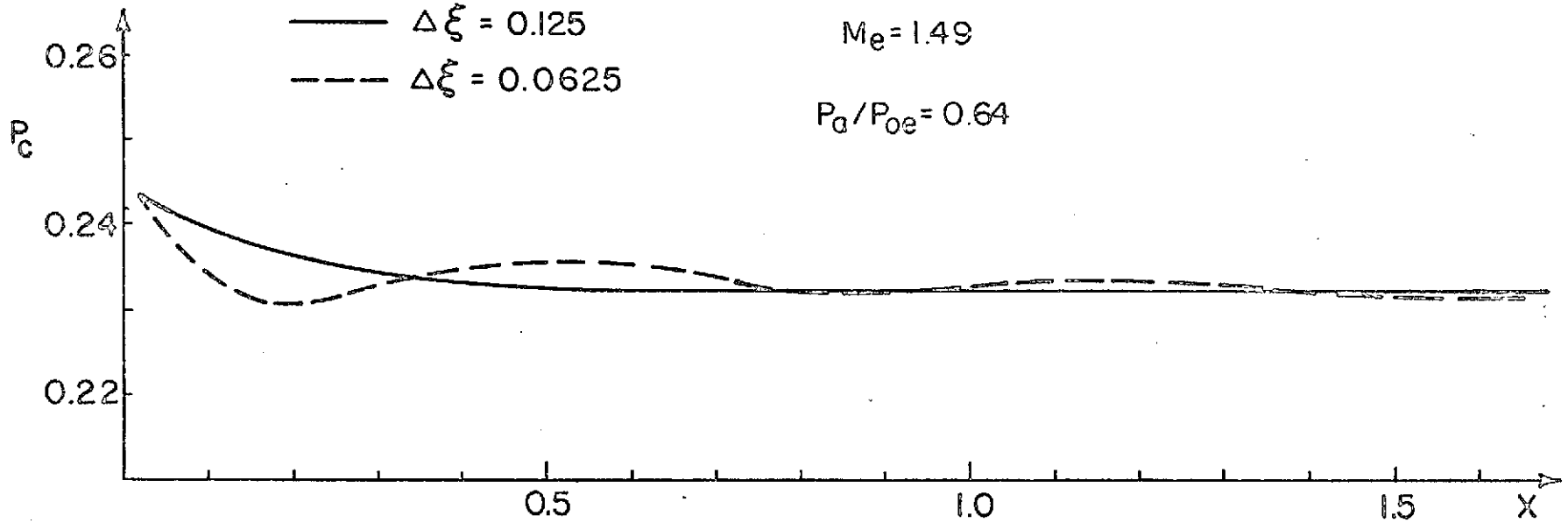

Figure 18 Centerline Pressure Distribution for Different Step Size $\Delta\xi$ at $M_e = 1.49$ and $p_a/p_{oe} = 0.64$

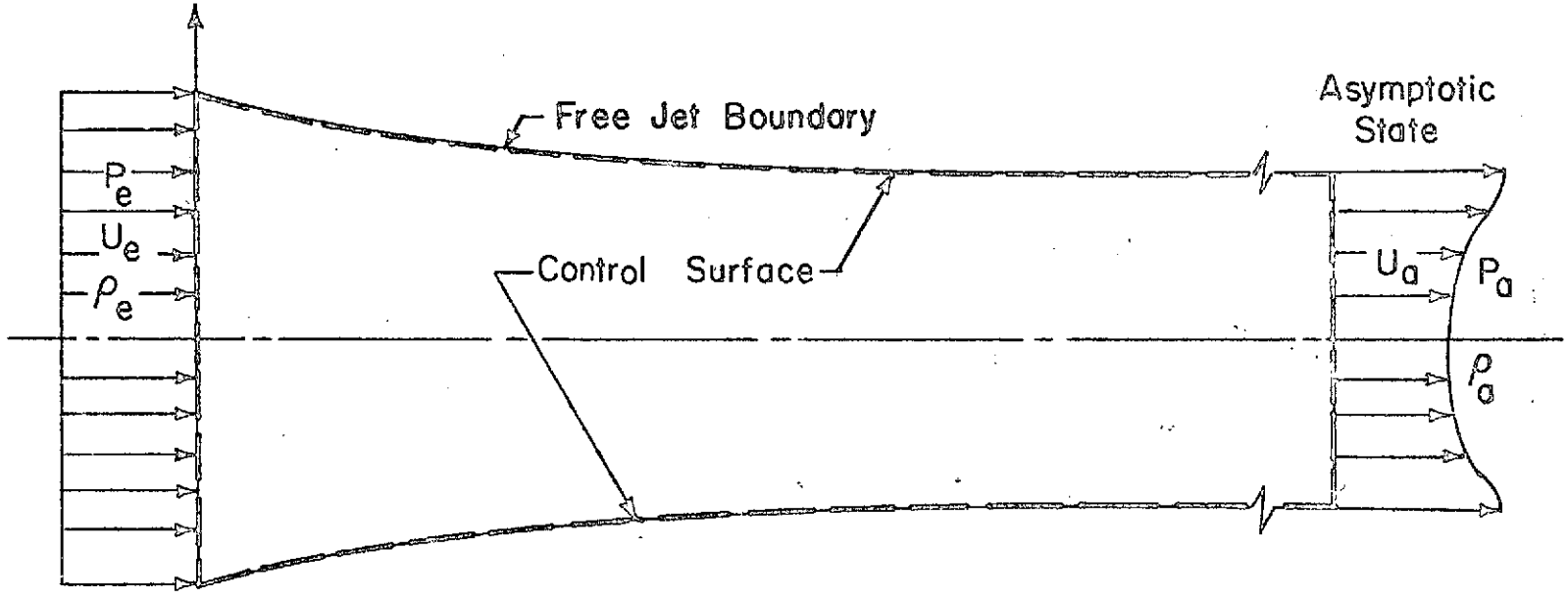

Figure 19 Control Volume for Axially Symmetric Flow

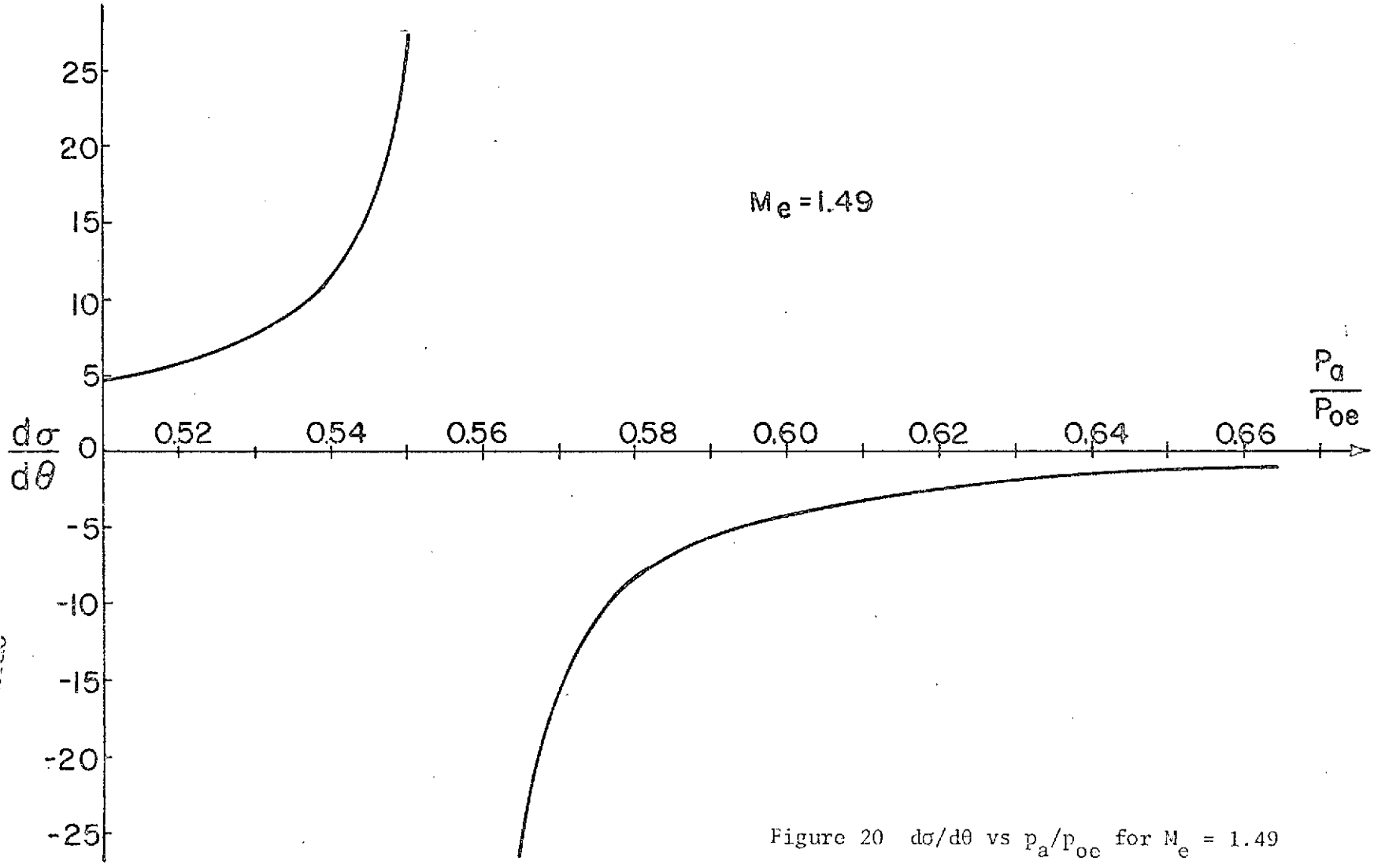

Figure 20 $d\sigma/d\theta$ vs p_a/p_{oe} for $M_e = 1.49$

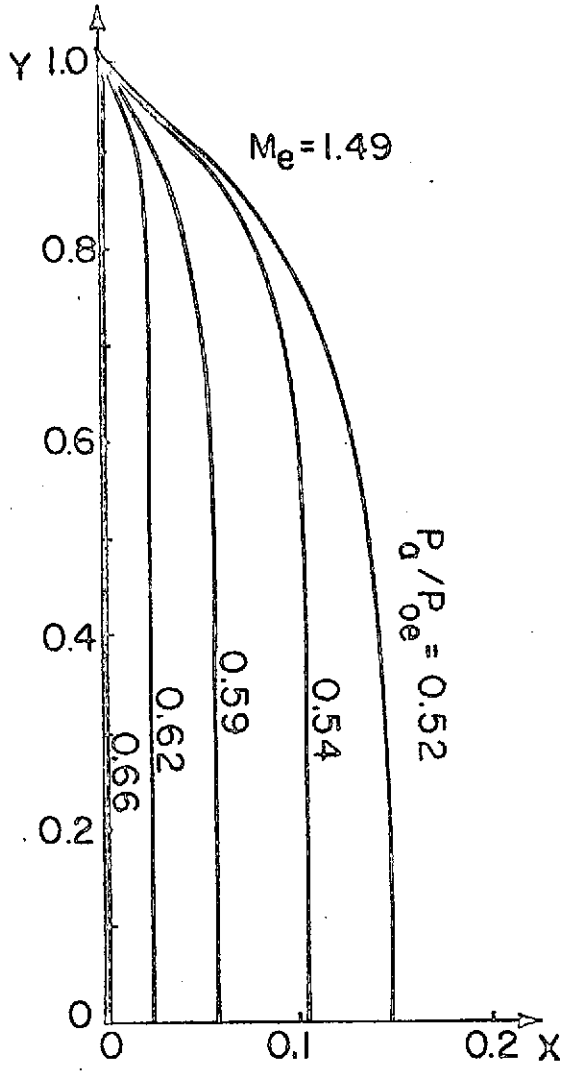

Curved Shock Profile

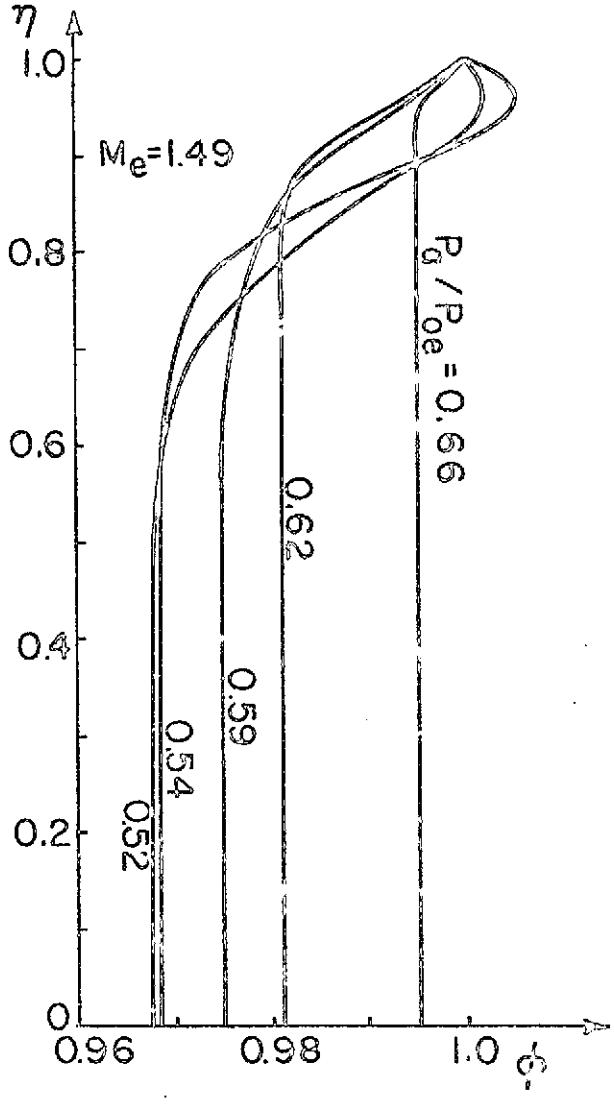

Asymptotic Velocity Profile

Figure 21 Curved Shock and Asymptotic Velocity Profiles of Axially Symmetric Flow for M_e = 1.49

Table 1 C Values for Different Flow Conditions

M_e = 1.49		M_e = 2.0		M_e = 3.0		M_e = 4.0		M_e = 5.0	
p_a/p_{oe}	C	p_a/p_{oe}	C	p_a/p_{oe}	C	p_a/p_{oe}	C	p_a/p_{oe}	C
0.50	0.6067	0.42	1.4038	0.22	2.2994	0.07	1.0426	0.044	2.8406
0.51	0.8410	0.43	1.5455	0.23	2.7216	0.08	1.5317	0.045	3.1077
0.52	1.0352	0.44	1.6923	0.24	3.3338	0.09	2.0884	0.046	3.4330
0.53	1.2121	0.45	1.8484	0.25	4.3267	0.10	2.9865	0.047	3.8388
0.54	1.3826	0.46	2.0191	0.26	6.2304	0.11	5.2914	0.048	4.3604
0.55	1.5540	0.47	2.2111	0.27	11.4360	0.12	31.4710	0.049	5.0564
0.56	1.7331	0.48	2.4348	0.28	72.0330	0.121	56.700	0.050	6.0341
0.57	1.9276	0.49	2.7047					0.051	7.5120
0.58	2.1480	0.50	3.0427					0.052	10.0170
0.59	2.4097	0.51	3.4832					0.053	15.2500
0.60	2.7373	0.52	4.0826					0.054	32.9090
0.61	3.1709	0.53	4.9463					0.0546	54.6450
0.62	3.7792	0.54	6.2994						
0.63	4.6953	0.55	8.7246						
0.64	6.2289	0.56	14.3560						
0.65	9.3159	0.57	40.3770						
0.66	18.7750	0.573	75.8470						
0.668	77.1230								

REFERENCES

1. Shapiro, A. H., The Dynamics and Thermodynamics of Compressible Fluid Flow, 1953, The Ronald Press Co., New York, Vol. 1.

2. Ferri, A., Elements of Aerodynamics of Supersonic Flows, The MacMillan Co., New York, 1949.

3. Chapman, A. J. and F. W. William, Introductory Gas Dynamics, Holt, Rinehart, and Winston, New York, 1971.

4. Chang, I. S., "Mach Reflection, Mach Disc, and the Associated Nozzle Free Jet Flows," Ph.D. Thesis, Department of Mechanical and Industrial Engineering, University of Illinois at Urbana-Champaign, Urbana, Ill., 1973.

5. Chow, W. L. and I. S. Chang, "Mach Reflection from Overexpanded Nozzle Flows," AIAA J., September 1972, Vol. 10, No. 9, pp. 1261-1263.

6. Chow, W. L. and I. S. Chang, "Mach Reflection Associated with Overexpanded Nozzle Free Jet Flows," paper to be published by AIAA J.

7. Bleakney, W. and A. H. Taub, "Interaction of Shock Waves," Rev. of Modern Physics, 1949, Vol. 21, No. 4, pp. 584-605.

8. Dorodnitzn, A. A., "On a Method of Numerical Solution of Some Nonlinear Problem of Aero-Hydrodynamics," Proc. Ninth International Cong. Appl. Mech., University of Brussels, 1957, Vol. 1, p. 485.

9. Belotserkovskii, O. M., "Flow past a Circular Cylinder with a Detached Shock," Doklady, Akad. Nauk SSSR. 1957, Vol. 113, No. 3, pp. 509-512 (Russian); M. D. Friedman, Trans. No. B-131.

10. Belotserkovskii, O. M., "Symmetric Flow about Blunt Bodies in a Supersonic Stream of a Perfect and Real Gas," Zh. Vychislitel'noi Mat. i. Mat. Fiz. 2, 1962, pp. 1062-1085; Trans. in USSR Comput. Math. and Math Phys., pp. 1272-1304.

11. Mel'nikov, D. A., "Reflection of Shocks from an Axis of Symmetry," Izv. AN SSSR, OTN, Mekhanika i mashinostroenie, 1962, No. 3.

12. Von Nuemann, J. and R. D. Richtmeyer, "A Method for Numerical Calculations of Hydrodynamic Shocks," J. of Appl. Phys., 1950, Vol. 21, p. 232.

13. Lax, P. D. and B. Wendroff, "Difference Schemes for Hyperbolic Equations with High Order of Accuracy," Commun. Pure. Appl. Math., 1964, Vol. 17, pp. 381-398.

14. Moretti, G. and M. Abbett, "A Time-Dependent Computational Method for Blunt Body Flows," AIAA J., December 1966, Vol. 4, No. 12, p. 2136.

15. Moretti, G. and G. Bleich, "Three-Dimensional Flow around Blunt Bodies," AIAA J., September 1967, Vol. 5, No. 19, p. 1577.

16. Geavalos, F. G., I. H. Edelfelt, and H. W. Emmons, "The Supersonic Flow about a Blunt Body of Resolution for Gases at Chemical Equilibrium," Proc. Ninth International Astronautical Congr., Amsterdam, 1958, Vol. 1, pp. 312-332.

17. Hayes, W. D. and R. F. Probstein, Hypersonic Flow Theory, Academic Press, Inc., New York, 1959.

18. Van Dyke, M. D. and H. D. Gordon, "Supersonic Flow Past a Family of Blunt Axisymmetric Bodies," NASA TR R-1, 1959.

19. Fuller, F. B., "Numerical Solutions for Supersonic Flow of an Ideal Gas around Blunt Two-Dimensional Bodies," NASA TN D-791, July 1961.

20. Inouye, M., J. V. Rakich, and H. Lomax, "A Description of Numerical Methods and Computer Programs for Two-Dimensional and Axisymmetric Supersonic Flow over Blunt-Nosed and Flared Bodies," NASA TN D-2970, August 1965.

21. Chow, W. L. and A. L. Addy, "Interaction between Primary and Secondary Streams of Supersonic Ejector Systems and their Performance Characteristics," AIAA J., April 1964, Vol. 2, No. 4, p. 686.

22. Bickley, W. G., "Formulae for Numerical Differentiation," Math. Gazette, October 1939, XXIII, pp. 352-359.

APPENDIX

FLOW WITH STRONG CURVED SHOCK WITH AXIALLY SYMMETRIC CONFIGURATION

The basic flow pattern of the axially symmetric flow within this flow regimeis similar to that of two-dimensional flow. The curved shock occurs at the exit of the nozzle and becomes a normal shock at the axis of symmetry. Behind the shock, the flow is rotational and bounded by a free jet boundary. Eventually this free jet flow reaches an asymptotic state at far down stream position ($x \to \infty$) where the pressure is constant. A schematic diagram depicting such a flow field is shown in Fig. 5 where x and y are interpreted as cylindrical coordinates.

A.1 BASIC RELATIONS GOVERNING THE FLOW

The governing relations are listed sequentially in the following sections.

A.1.1 Shock Relations

The governing shock equations are the same as those for two-dimensional flow. See Eqs. (2.1) through (2.5).

A.1.2 Free Jet Flow Region

For axially symmetric inviscid flow of a compressible fluid, the continuity and momentum principles can be given as:

$$\frac{\partial \rho u y}{\partial x} + \frac{\partial \rho v y}{\partial y} = 0 \tag{A.1}$$

$$\rho u \frac{\partial u}{\partial x} + \rho v \frac{\partial u}{\partial y} + \frac{1}{\kappa M_e^2} \frac{\partial p}{\partial x} = 0 \tag{A.2}$$

$$\rho u \frac{\partial v}{\partial x} + \rho v \frac{\partial v}{\partial y} + \frac{1}{\kappa M_e^2} \frac{\partial p}{\partial y} = 0 \tag{A.3}$$

The energy equation can be given as

$$\frac{DS}{Dt} = 0 \ . \tag{A.4}$$

The flow region is bounded by (1) a constant pressure jet boundary, (2) the upstream curved shock, and (3) the asymptotic state prevailing at far downstream position (i.e., $x \to \infty$).

The boundary condition for Eqs. (A.1), (A.2), and (A.3) are:

$p = p_a$ along the free jet boundary,

$u = u_s$, $v = v_s$, $p = p_s$, and $\rho = \rho_s$ along the curved shock,

$v = 0$, $\frac{\partial u}{\partial y} = 0$ at $y = 0$.

A.1.3 Constraining Condition at the Asymptotic State

Consider the control volume shown in Fig. 19. The continuity principle would yield

$$\int_0^{y_{aj}} \rho_a \, u_a \, y_a \, dy_a = \int_0^{y_e} \rho_e \, u_e \, y \, dy = \frac{1}{2} \tag{A.5}$$

and the x-momentum principle also gives

$$\int_0^{y_{aj}} \rho_a \, u_a^2 \, y_a \, dy_a + \frac{p_a \, y_e}{2\kappa \, M_e^2} = \frac{p_e \, y_e}{2\kappa \, M_e^2} + \rho_e \, u_e^2 \, \frac{y_e^2}{2} \tag{A.6}$$

which can be rewritten as

$$\int_0^{y_{aj}} \rho_a \, u_a^2 \, y_a \, dy_a = \frac{1}{2}\left(1 - \frac{p_a - 1}{\kappa \, M_e^2}\right). \tag{A.7}$$

After introducing ρ_{aj}, u_{aj}, and y_{aj} as reference quantities for the integrands in Eqs. (A.5) and (A.7) and defining $\phi = u_a/u_{aj}$ and $\eta = y/y_{aj}$,

these equations become

$$\rho_{aj}\, u_{aj}\, y_{aj} \int_0^1 \frac{\rho_a}{\rho_{aj}}\, \phi\eta \;\; d\eta = \frac{1}{2} \tag{A.8}$$

$$\rho_{aj}\, u_{aj}^2\, y_{aj} \int_0^1 \frac{\rho_a}{\rho_{aj}}\, \phi^2 \;\; \eta\, d\eta = \frac{1}{2}\left(1 - \frac{p_a - 1}{\kappa\, M_e^2}\right). \tag{A.9}$$

Upon combining Eqs. (A.8) and (A.9), one obtains

$$\int_0^1 \frac{\rho_a}{\rho_{aj}}\, \phi\, \eta \left(\phi - \frac{1 - \frac{1}{\kappa\, M_e^2}\,(p_a - 1)}{\kappa\, M_e^2}\right) d\eta = 0 \tag{A.10}$$

A method similar to the two-dimensional flow method has been applied to calculate this flow case. Detailed calculation procedures will be discussed in the following sections.

A.2 ASYMPTOTIC STATE

Since the solution of the problem relies on the establishment of the asymptotic flow profile, a detailed examination of the conditions imposed on such an asymptotic flow state is, therefore, necessary.

Under the asymptotic flow condition, the slope of the velocity profile is precisely the vorticity of the flow. A study of the vorticity generated by the shock at the corner of the nozzle would also yield the slope of the profile of the jet boundary streamline at the asymptotic state.

A.2.1 Vorticity at the Jet Boundary Streamline

Referring to Fig. 7, the continuity equation and the equation of motion in the streamline coordinate system are (in dimensional form):

$$\frac{1 - M_e^2}{q} \frac{\partial q}{\partial s} + \frac{\partial \theta}{\partial n} = - \frac{\sin \theta}{y} \tag{A.11}$$

$$q \frac{\partial q}{\partial s} = - \frac{1}{\rho} \frac{\partial p}{\partial s} \tag{A.12}$$

$$\rho q^2 \frac{\partial \theta}{\partial s} = - \frac{\partial p}{\partial n} . \tag{A.13}$$

The vorticity can be expressed as

$$\omega = \frac{\partial q}{\partial n} - q \frac{\partial \theta}{\partial s} = \frac{p}{\rho q R} \frac{\partial S}{\partial n} . \tag{A.14}$$

For a jet boundary streamline at the corner of the nozzle, Eq. (A.11) can be written as

$$\frac{\partial \theta}{\partial n} = - \frac{\sin \theta}{y} \text{ as } \frac{\partial p}{\partial s} = 0. \tag{A.15}$$

At asymptotic state, the relation between the vorticity and the slope of velocity profile can be expressed as

$$\omega_a = \left. \frac{\partial q}{\partial n} \right|_a = \frac{u_{aj}}{y_{aj}} \frac{\partial \phi}{\partial \eta} . \tag{A.16}$$

The vorticity at the shock can be written as

$$\omega_s = \left. \frac{p}{\rho q R} \frac{\partial S}{\partial n} \right|_s = \frac{p}{\rho q R} \left(\frac{dS}{d\sigma} \frac{d\sigma}{d\theta} \frac{\partial \theta}{\partial n} \right)_s . \tag{A.17}$$

For axially symmetric flow, the vorticity along each streamline is not constant. It is proportional to the pressure moment y p relative to the axis of symmetry. Thus, along the constant pressure free jet boundary, the vorticity at the asymptotic state can be related to the vorticity at the shock by

$$\omega_a = \omega_s \frac{y_a}{y_s} = \frac{p}{\rho q R} \left(\frac{dS}{d\sigma} \frac{d\sigma}{d\theta} \frac{\partial \theta}{\partial n} \right) \frac{y_a}{y_s} = \left. \frac{\partial q}{\partial n} \right|_a . \tag{A.18}$$

The change of entropy with respect to the shock angle $dS/d\sigma$ can be obtained from the following relations:

$$\frac{dS}{d\sigma} = \frac{4R\kappa}{(\kappa - 1)(\kappa + 1)} \left\{ \frac{M_e^2 \sin\sigma \cos\sigma}{\frac{2\kappa}{\kappa + 1} M_e^2 \sin^2\sigma - \frac{\kappa - 1}{\kappa + 1}} \right.$$

$$\left. - \frac{\cos\sigma/(M_e^2 \sin^3\sigma)}{\frac{2}{(\kappa + 1) M_e^2 \sin^2\sigma} + \frac{\kappa - 1}{\kappa + 1}} \right\}. \qquad (A.19)$$

Taking the derivative of Eq. (2.2), one obtains

$$\frac{d\sigma}{d\delta} = - \frac{1/\sin^2\delta}{\frac{1}{\cos^2\sigma}\left(\frac{\kappa + 1}{2} \frac{M_e^2}{M_e^2 \sin^2\sigma - 1} - 1\right) - \frac{(\kappa + 1) M_e^4 \sin^2\sigma}{(M_e^2 \sin^2\sigma - 1)^2}} ; \qquad (A.20)$$

thus, the slope of the asymptotic velocity profile can be related to the shock angle, shock turning angle, and the asymptotic free jet height by

$$\left.\frac{\partial\phi}{\partial\eta}\right|_{\eta=1} = \frac{p_s \sin\delta}{\rho_s q_s q_{aj}} \frac{4\kappa}{(\kappa - 1)(\kappa + 1)}$$

$$\cdot \left(\frac{M_e^2 \sin\sigma \cos\sigma}{\frac{2\kappa}{\kappa + 1} M_e^2 \sin^2\sigma - \frac{\kappa - 1}{\kappa + 1}} - \frac{\frac{\cos\sigma}{M_e^2 \sin^3\sigma}}{\frac{2}{(\kappa + 1) M_e^2 \sin^2\sigma} + \frac{\kappa - 1}{\kappa + 1}} \right)$$

$$\cdot \left(\frac{\frac{1}{\sin^2\delta}}{\frac{1}{\cos^2\sigma}\left(\frac{\kappa + 1}{2} \frac{M_e^2}{M_e^2 \sin^2\sigma - 1} - 1\right) - \frac{(\kappa + 1) M_e^4 \sin^2\sigma}{(M_2^2 \sin^2\sigma - 1)^2}} \right)$$

$$\cdot \frac{y_{aj}^2}{y_s^2} = F(M_e, \sigma, \delta, y_{aj}) \qquad (A.21)$$

It should be pointed out that at certain pressure ratios, $d\sigma/d\delta$ in Eq. (A.20) becomes undefined (i.e., $d\sigma/d\delta = \pm\infty$) as shown in Fig. 20. This implies that the slope of the asymptotic velocity profile is also undefined. However, when the pressure ratios are different from that particular pressure ratio, present calculations are successful and the corresponding shock profiles can be computed.

A.2.2 Velocity Profile at the Asymptotic State

The velocity profile ϕ in Eq. (A.10) should satisfy the conditions of:

(1) At $\eta = 0$:

$$\phi = \phi_c = \frac{u_{ac}}{u_{aj}} \text{ and } \frac{d\phi}{d\eta} = 0 \ .$$

(2) At $\eta = 1$:

$$\phi = 1 \text{ and } \frac{d\phi}{d\eta} = F\ (M_e,\ \sigma,\ \delta,\ y_{aj}) \ .$$

A similar velocity profile has been selected as

$$\phi = A + B \text{ erf } [C\ (1 - \eta^2)] + D \text{ erf } [C\ (1 - \eta^4)] \ . \qquad (A.22)$$

Since the boundary condition $d\phi/d\eta\big|_{\eta=1}$ is related to the asymptotic free jet boundary height y_{aj}, iteration must be applied to determine the values of those coefficients and the free jet boundary height, y_{aj}.

A.2.3 Corresponding Upstream Shock Profile

After the asymptotic free jet height y_{aj} and its detailed profile have been established, the corresponding curved shock configuration can be determined through the following consideration.

If one carries out the integration

$$\int_0^{y_a} \rho_a \, u_a \, y \, dy$$

along the asymptotic profile, continuity principle would imply that the fluid assuming the position y_a at the asymptotic section would have passed through the shock at height y_s which is equal to

$$y_s = 2\left(\int_0^{y_a} \rho_a \, u_a \, y \, dy\right)^{1/2} . \tag{A.23}$$

Since the velocity of the fluid at y_a has a known value of ϕ_a, its stagnation pressure p_{oa} can be found from

$$\frac{p_{oa}}{p_a} = \left(\frac{1}{1 - C_{aj}^2 \, \phi_a^2}\right)^{(\kappa/\kappa-1)} . \tag{2.32}$$

The ratio of the stagnation pressure across the shock at y_s can be related through the shock wave angle σ by

$$\frac{\left(\dfrac{\frac{\kappa+1}{2} M_e^2 \sin^2\sigma}{1 + \frac{\kappa+1}{2} M_e^2 \sin^2\sigma}\right)^{(\kappa/\kappa-1)}}{\left(\dfrac{2\kappa}{\kappa+1} M_e^2 \sin^2\sigma - \dfrac{\kappa-1}{\kappa+1}\right)^{(1/\kappa-1)}} = \frac{p_{oa}}{p_{oe}} = \frac{p_{oa}}{p_a}\frac{p_a}{p_{oe}} . \tag{A.24}$$

The wave angle σ, thus, can be found as a function of any position y_s along the shock.

The calculated shock profiles and asymptotic velocity profiles for $M_e = 1.49$ at different pressure ratios are given in Fig. 20.

It should be noted that at low pressure ratios, the maximum asymptotic velocity is not at free jet boundary. This is, of course, a result of the positive vorticity occurring at the corner of the nozzle under these specific pressure ratios.

VITA

Tso-Shin Shih was born on [redacted]. He received the degree of Bachelor of Science in Mechanical Engineering from the National Taiwan University, Taipei, Taiwan, in July 1964 and the degree of Master of Science in Mechanical Engineering from the University of North Dakota, Grand Forks, North Dakota, in January 1969.

He entered the University of Illinois at Urbana-Champaign for his doctoral degree studies in September 1969. He held a teaching assistantship for one year and a research assistantship, sponsored by the National Aeronautics and Space Administration, Lewis Laboratory, Cleveland, Ohio, for five years.